Title
Ligand- and oxygen-isotope-exchange pathways of geochemical interest

Journal
Environmental Chemistry, 12(1)

ISSN
1448-2517

Author
Casey, William H

Publication Date
2015

DOI
10.1071/en14043

Peer reviewed

RESEARCH FRONT

CSIRO PUBLISHING

Environ. Chem. **2015**, *12*, 1–19
http://dx.doi.org/10.1071/EN14043

Research Paper

Ligand- and oxygen-isotope-exchange pathways of geochemical interest

William H. Casey

Department of Chemistry and Department of Geology, University of California, 1 Shields Lane, Davis, CA 95616, USA. Email: whcasey@ucdavis.edu

Environmental context. Most chemical processes in water are either ligand- or electron-exchange reactions. Here the general reactivity trends for ligand-exchange reactions in aqueous solutions are reviewed and it is shown that simple rules dominate the chemistry. These simple rules shed light on most molecular processes in water, including the uptake and degradation of pesticides, the sequestration of toxic metals and the corrosion of minerals.

Abstract. It is through ligand-exchange kinetics that environmental geochemists establish an understanding of molecular processes, particularly for insulating oxides where there are not explicit electron exchanges. The substitution of ligands for terminal functional groups is relatively insensitive to small changes in structure but are sensitive to bond strengths and acid–base chemistry. Ligand exchanges involving chelating organic molecules are separable into two classes: (i) ligand substitutions that are enhanced by the presence of the chelating ligand, called a 'spectator' ligand and (ii) chelation reactions themselves, which are controlled by the Lewis basicity of the attacking functional group and the rates of ring closure. In contrast to this relatively simple chemistry at terminal functional groups, substitutions at bridging oxygens are exquisitely sensitive to details of structure. Included in this class are oxygen-isotope exchange and mineral-dissolution reactions. In large nanometer-sized ions, metastable structures form as intermediates by detachment of a surface metal atom, often from a underlying, highly coordinated oxygen, such as μ_4-oxo, by solvation forces. A metastable equilibrium is then established by concerted motion of many atoms in the structure. The newly undercoordinated metal in the intermediate adds a water or ligand from solution, and protons transfer to other oxygens in the metastable structure, giving rise to a characteristic broad amphoteric chemistry. These metastable structures have an appreciable lifetime and require charge separation, which is why counterions affect the rates. The number and character of these intermediate structures reflect the symmetry of the starting structure.

Received 28 February 2014, accepted 27 May 2014, published online 7 January 2015

Introduction

Interfacial reactions that concern environmental geochemists fall into simple classes: they are either ligand-exchange reactions, electron-exchange reactions or a mixture of the two. Ligand-exchange reactions include dissolution of a mineral, oxygen-isotope exchanges, adsorbate uptake and reconstruction of the surface into a lower-energy state. Molecular questions about the pathways for these ligand-exchange reactions cannot be answered uniquely with bulk experiments. In these experiments it is rarely clear which functional groups are present at the surface, or how they are arranged, or how they interact with each other and with solutes as the key bonds are activated.

At the size scale of nanometres, much can be learned from the study of large metal-oxide ions that dissolve intact to make a monospecific solution. The structure of these clusters can be known with great confidence and they can be made relatively inert and synthesised with targeted heteroatom substitutions so that experiments to follow bond ruptures and dissociations can be conducted with great sensitivity. Here the results describing such reactions are reviewed and an attempt to draw conclusions for the extended surfaces, where molecular details are difficult to acquire, is made.

The enormous body of literature on molecules of varying denticity and size undergoing ligand-exchange and ligand-addition reactions is drawn upon and oversimplified.[1,2] An understanding of these reactions, and extrapolation to the environment, must be made inductively. An understanding derived from simple systems and solutions must be extended to the complex processes of environmental chemistry in soils. The extrapolation can be frustratingly qualitative, but nevertheless these ligand-exchange reactions, particularly at mineral surfaces, retard the ecotoxicity of pollutants, often by reducing the toxicant lability or by making them susceptible to degradation by other processes, such as microbial degradation or photolysis.

Simple reactivity trends for ligand- and oxygen-isotope exchanges

Formalism

Most metals in aqueous solutions of interest to environmental chemists are coordinatively saturated. Here saturated is meant in the sense of Pauling's First Rule, relating ionic radius to oxygen packing. Most metals in water have the maximum number of coordinated atoms given by their radius ratios – exceptions certainly exist for highly covalent materials (e.g. Pt^{II}, Nb^{V}), and some are discussed below, but most materials near the Earth's surface are oxides with a metal that has a fixed coordination or slightly variable number. In sharp contrast, the coordination

Table 1. Metal–oxygen distances (M–O, Å) for hydrated cations, oxide minerals and orthosilicate minerals (see Casey[104] for sources)

The distances are similar because the metal coordination number in the solid is similar to that in the solute. One exception is Zn^{II}, which is hexa-coordinated in the solute but tetrahedrally coordinated in the oxide and silicate minerals

Ion	M–O	Oxide	M–O	Silicate	M–O
$[Ca(H_2O)_6]^{2+}$	2.39–2.46	CaO	2.405	Ca_2SiO_4	2.346–2.392
$[Mg(H_2O)_6]^{2+}$	2.10	MgO	2.11	Mg_2SiO_4	2.101–2.127
$[Be(H_2O)]_4^{2+}$	1.67	BeO	1.649	Be_2SiO_4	1.645
$[Zn(H_2O)_6]^{2+}$	2.08–2.17	ZnO	1.95	Zn_2SiO_4	1.92
$[Mn(H_2O)_6]^{2+}$	2.18–2.20	MnO	2.22	Mn_2SiO_4	2.185–2.227
$[Co(H_2O)_6]^{2+}$	2.05–2.08	CoO	2.13	Co_2SiO_4	2.123–2.134
$[Ni(H_2O)_6]^{2+}$	2.04–2.10	NiO	2.095	Ni_2SiO_4	2.076–2.102
$[Al(H_2O)_6]^{3+}$	1.87–1.97	α-Al_2O_3	1.86–1.97		

number of the oxygens changes dramatically during common aqueous reactions. Magnesium in periclase or in the brucitic layer of a clay, for example, is coordinated to six oxygens both in the bulk and at the interface (Table 1). The magnesium in the $[Mg(OH_2)_6]^{2+}$ ion released by dissolution of these minerals is also coordinated to six oxygens and in all cases the bond lengths are near 2.1 Å. In contrast the coordination numbers of the oxygens vary from one to six at simple kink sites on the surface of MgO (in the bulk structure they are all six-coordinated) and these all convert into singly coordinated oxygens in $[Mg(OH_2)_6]^{2+}$ as the solid dissolves. Thus, transfer of a metal from a solid to solution is a ligand-exchange process where bridging oxygens are replaced with terminal oxygens. The number of coordinated ligands is usually preserved.

Exceptions are not hard to find. Aluminium can exist in four-, five- or six-coordination in solids and the aluminium ion changes coordination from six in $[Al(OH_2)_6]^{3+}$ to five in $[AlOH(OH_2)_4]^{2+}$ to four in the $[Al(OH)_4]^-$ ion[3] as the pH rises. Aluminium is both four- and six-coordinated in the oligomer $[AlO_4Al_{12}(OH)_{24}(OH_2)_{12}]^{7+}$. Boric acid $[B(OH)_3]^0$ has boron coordinated to three oxygens but adds a fourth when it becomes the borate ion: $[B(OH)_4]^-$. The metal Si^{IV} can be induced to change it's coordination number from four to five to six by ligation to simple sugars.[4] Ferric iron can be tetrahedrally coordinated in some oxide minerals but is octahedrally coordinated in most aqueous ions at near-neutral or slightly acidic solutions usually found in nature.

Most, but not all, metals happily retain their coordination number when they transfer from minerals to mineral surfaces to aqueous ions. To understand ligand-exchange kinetics, one needs to focus on the changing coordination of oxygens. In the formalism of inorganic chemistry, atoms that bridge '*i*' metal atoms are denoted 'μ_i' and non-bridging ligands bonded by '*i*' atoms are denoted '$^i\eta$' and this formalism is used throughout this article. Thus, for example, the $[AlO_4Al_{12}(OH)_{24}(OH_2)_{12}]^{7+}$ ion has a structure that is familiar to chemists as the ε-isomer of the Baker–Figgis–Keggin class (Fig. 1, top). The ion has four μ_4-O in the centre of the molecule, 24 μ_2-OH bridges and 12 $^1\eta$-OH_2 or bound waters. As a second example, the beautiful iron tetramer shown in Fig. 1 (centre)[5] has two μ_2-OH bridges in the centre, four bound waters or η-OH_2, two μ_3-O from the aminocarboxylate ligands, four μ_3-N and eight μ_2-O from the carboxylate ligands. Waters bound to metals in aqueous solutions are virtually never bridging groups and they bond by single sigma bonds. Therefore, one can dispense with the superscripts for ligated waters and just call them η-OH_2 or 'bound waters' instead of the more cumbersome $^1\eta$-OH_2. Finally, in Fig. 1 (bottom) is shown the various oxygens in the decaniobate ion $[Nb_{10}O_{28}]^{6-}$, which is examined in greater detail later.

Exchanging bound waters

The most important time scale for aqueous environmental geochemists to understand is the movement of a water molecule from the inner-coordination sphere of a metal to the bulk solution. For most aqueous reactions, even those where the incoming ligand is not another water molecule, the rate-controlling step is the movement of the metal-bound solvation water to get out of the way. This two-step pathway is called the Eigen–Wilkins–Tamm pathway and is so general as to become a rule of thumb for aqueous processes. Thus rates of exchanges of bound waters give general information about a host of other ligand-exchange reactions. The rates reflect the strength of the metal–oxygen bond and span a range of $\sim 10^{20}$ at room temperature for octahedral metal ions (Fig. 2). Some ions like $[Cs(OH_2)_{8-9}]^{3+}$, exchange their bound waters upon every collision with bulk waters. In contrast, $[Ir(OH_2)_6]^{3+}$ exchanges a bound water for a bulk water every 200 years[6] at room temperature.

Octahedrally coordinated di- and trivalent metals provide the best examples because these metals have an interesting acid–base chemistry in natural waters. Small highly charged metals with strong bonds to the solvation waters, like Al^{III}, tend to have slower rates of exchange of bound waters than larger metals with lower charge, like Mg^{II}. The charge density of the ion controls much, but not all, of the kinetics of ligand substitution and covalency is important for metals deeper in the periodic table, as is discussed below, and transition metals with directional bonding.

Monovalent metal ions exchange waters much faster than most divalent metal ions, and these themselves exchange much faster than most trivalent ions. Tetra-, penta and hexavalent metal ions usually no longer have bound waters unless they are quite large, like Th^{IV}, but either have bound hydroxides, like silicic acid, $[Si(OH)_4]^0$, a mix of hydroxide and oxo ligands, as in phosphoric acid, $[PO(OH)_3]$ or oxo ligands only, as in the sulfate ion, SO_4^{2-}. The metal charge and size controls the bond strengths and acid–base chemistry of the bound waters, and thus is manifested in the rates of ligand substitution.

For transition metals, rates scale with parameters that describe the d-electron structure, such as the crystal-field or ligand-field energies and these are non-linear with electron count (Fig. 3). Solvated metals with symmetric d-electron configurations, like d^5 Mn^{II} in the $[Mn(OH_2)_6]^{2+}$ ion, or d^{10} Zn^{II} in the $[Zn(OH_2)_6]^{2+}$ ion, have much more rapid rates of exchange relative to d^8 Ni^{II} in the $[Ni(OH_2)_6]^{2+}$ ion (Fig. 3). Rates for transition metals tend to slow within a Group as one goes deeper, hence rates around Co^{III} are slow but faster than around Rh^{III} and these are faster than rates around Ir^{III}. This trend in reactivity is dependable, and of course is expressed to different extents for second- and third-row transition metals. Rates are very slow in the spin-paired d^6 $[Co(OH_2)_6]^{3+}$, $[Rh(OH_2)_6]^{3+}$ and $[Ir(OH_2)_6]^{3+}$ because distortion to form an activated state requires much energy; the low-spin configuration is very stable. If one can add a ligand that disrupts the low-spin d^6 electronic configuration, the rates accelerate dramatically but these ligands are not geochemically common. Even a very strong ligand in nature, such as CN^-, is usually present in natural waters at concentrations of 10^{-7} M or less. Water molecules, however, are present at concentrations of 55.56 M. Many solid reviews of this subject exist.[6–9]

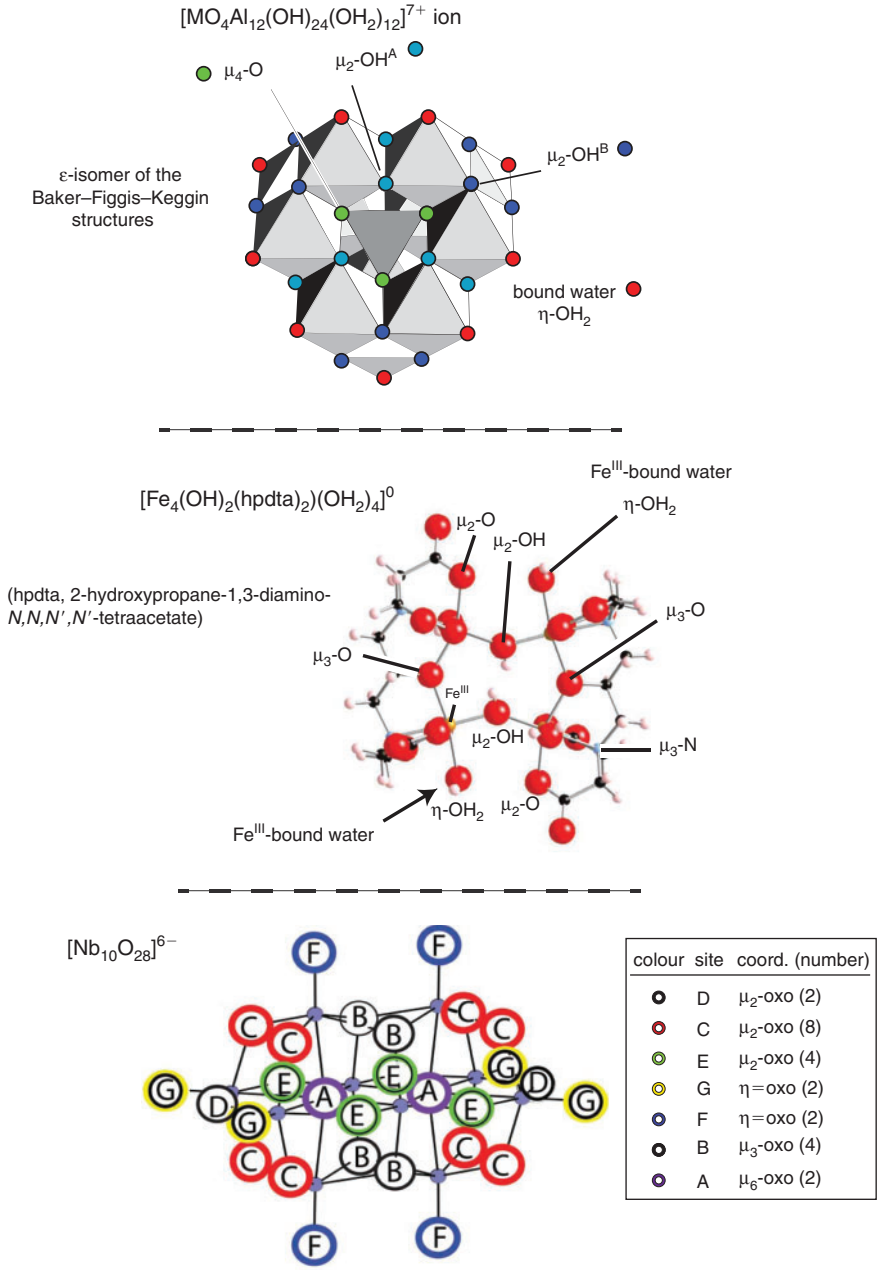

Fig. 1. The coordination number of oxygens commonly change in aqueous reactions, so it is useful to have a formalism that describes the coordination easily. (top) The $[MO_4Al_{12}(OH)_{24}(OH_2)_{12}]^{7+/8+}$ cation (top) forms in the structure of the ε-isomer of the Baker–Figgis–Keggin class, with four μ_4-oxo in the centre of the molecule (green), 24 μ_2-OH bridges in two sets (blue) and 12 η-OH_2 or bound waters (red). The metal substitution of Ga^{III} or Ge^{IV} for Al^{III} is exclusively in the central MO_4 site. (middle) A Fe^{III} tetramer has oxygens in red as two μ_2-OH bridges, four bound waters (η-OH_2), two μ_3-O from the aminocarboxylate ligands, four μ_3-N shown in light blue and eight μ_2-O from the carboxylate ligands. (bottom) The decametalate class of anions, here as a decaniobate, have three metal positions and seven structurally distinct oxygens. A $Ti^{IV} \rightarrow Nb^{V}$ substitution is possible in the central metal site, yielding $[Nb_{10}O_{28}]^{6-}$, $[TiNb_9O_{28}]^{7-}$ and $[Ti_2Nb_8O_{28}]^{8-}$ versions. The legend to this last bottom figure has the number of the various oxygens shown next to the abbreviation and coordination number. Thus there are eight 'C' sites in the molecule and these are all μ_2-O bridges.

Scaling to large dimensions

As stated above, even such odd reactions as mineral dissolution are really ligand-exchange reactions. In Fig. 4, the rates of dissolution of simple oxide and orthosilicate minerals are correlated, as well as the adsorption of metals to the alumina surface, to the rates of water exchange around the corresponding ion in solution. These are all ligand-exchange reactions but differ vastly in speed. Thus, for example, the dissolution rate of forsterite (Mg_2SiO_4) when the surface is fully protonated is plotted against the rates of exchange of a bound water between the

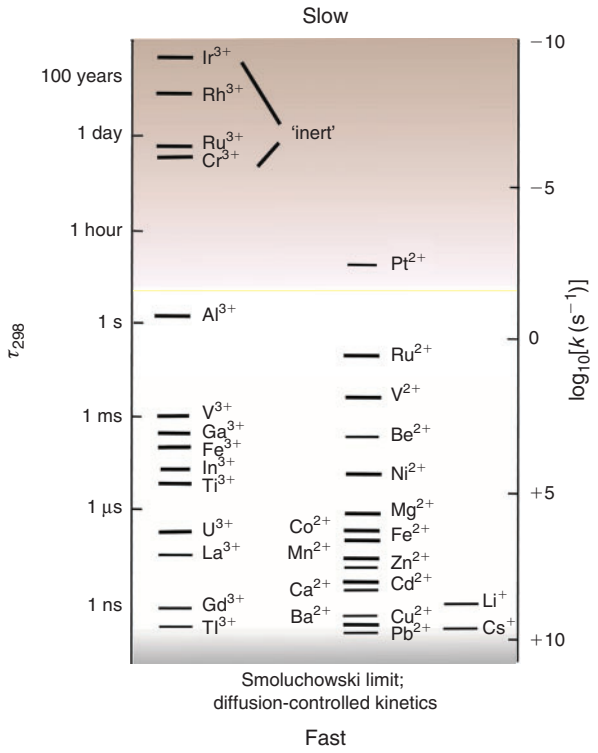

Fig. 2. Characteristic half-lives (τ_{298}) at 298 K and pseudo-first-order rate coefficients (k_{298}) for exchange of a water molecule bound in the inner-coordination sphere of a hydrated metal with a water molecule in bulk solution. $\tau_{298} = (\ln 2)/k_{298}$ (adapted from Casey and Swaddle[62] and Helm and Merbach[6]). The most rapid rates in water are controlled by diffusion, which is called the Smoluchowski limit, where every collision causes an exchange event.

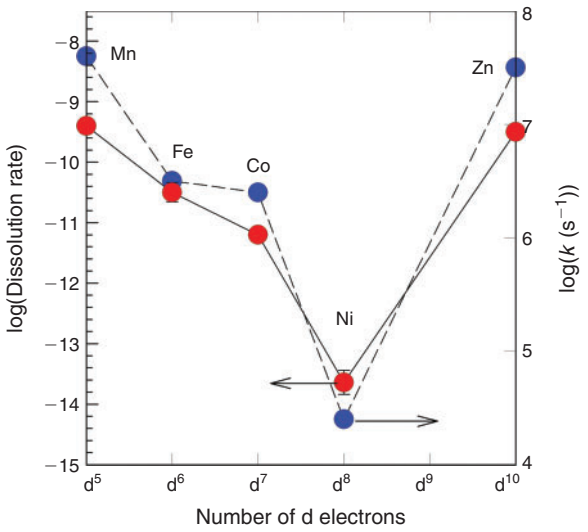

Fig. 3. The variation in dissolution rates of simple orthosilicate minerals faithfully reproduces the trends expected for first-row transition metal ions. Here the blue symbols and right-hand axis correspond to the rate coefficient for exchange of a bound water from around an ion (e.g. $[Ni(OH_2)_6]^{2+}$) and the red symbols and left-hand axis correspond to dissolution rates at pH = 2 of the corresponding orthosilicate mineral (e.g. liebenbergite, Ni_2SiO_4).[105,113]

$[Mg(OH_2)_6]^{2+}$ ion and bulk solution. As one can see, the correlation is direct (see also Fig. 3), but of course does not mean that the dissolution rates, which are slow, are controlled by rates of water exchanges, which are fast. This plot tells environmental chemists and geochemists that the same variables that affect the rates of ligand exchange around octahedrally coordinated metals in simple ions also affect the ligand-exchange reactions that dissolve a monoatomic step at a mineral surface or in a surface complex that has a similar general coordination chemistry. This reactivity trend can be ruined, of course, if the material has a robust, inert polymeric fabric that resists hydrolysis and dissociation, such as a silicate chain or framework, but this trend is a good starting place. It can be similarly ruined if the dissolution rate is not controlled by rates of ligand-exchange reactions affecting metal-oxide bonds, such as if the kinetics are controlled by solute diffusion instead of slow bond ruptures.

So how do rates of exchange of bound waters vary as one goes from simple monomer ions to mineral surfaces? Here is an environmental question of the highest priority and, until this last decade, the answer to this question was unknown. However there have been several studies recently that specifically address the role that oxide structure size plays in affecting the rates of exchange of bound waters from a solvated metal. The efforts have been both experimental and theoretical and are summarised in Fig. 5 where rates of exchange of bound waters are shown for simple monomer ions, intermediate-sized metal-oxide structures and huge nanometre-sized structures that have isolated bound waters, such as the enormous $Mo_{72}Fe_{30}$ Keplerate ion with 300 atoms. The plot also includes rates calculated for surface sites exposed on aluminium hydroxide minerals. These points are particularly important because they show that the simulations can find rates that are credible for exposed bound waters. Dynamic simulation methods called 'rare-event' methods are key because exchange of a terminal ligand is still too slow for direct counting of events in a computer (see Stack et al.[10]). These techniques accelerate and sample the process, and give credible results,[11] but the use of dynamic methods is essential.[10] Static ab initio calculations are too sensitive to details of the hydrogen-bonding structure of the nearby solvent to be useful for dynamic reactions like exchanges at mineral interfaces[12,13] that are central to environmental aqueous chemistry.

Rates of exchange of bound waters tend not to differ much for a given metal with molecular size unless the change in size is accompanied by a reduction in the average charge density, or metal–oxygen bond strengths. The rates of exchange of waters from $>Fe^{III}–OH_2$ functional groups on the Keplerate ion, for example, are much more rapid than for the $[Fe(OH_2)_6]^{3+}$ ion, but they are close to the rates observed for other molecules that have similar charge densities, like Fe-aminocarboxylate and Fe–edta (edta, ethylenediaminetetraacetic acid) complexes.[5,14] For heterogeneous oxide structure, bonding must be understood at the functional-group level but size itself isn't important unless there is a steric hindrance that comes with the functional group. The rates of exchange of the bound-water functional groups, in this case the $>Co^{II}–OH_2$ on a nanometre-sized ion having the stoichiometry of $[Co_4(H_2O)_2(P_2W_{15}O_{56})_2]^{16-}$, is very close to the values for the $[Co(OH_2)_6]^{2+}$ ion. In the large structure, the cobalts are organised into a brucite-like layer sandwiched between two large polyoxometalate ions. Their local bonding environment is controlled by the layered structure and is not dramatically affected by the dense and dissimilar tungstate groups.[15,16] Charge densities are important, not necessarily size.

At surfaces there are often reduced charge densities on the metals, resulting in the relaxation of metal–oxygen bonding at the mineral–solution interface and rapid rates of exchange.[11] Wang et al.[11] used the measured values on a series of

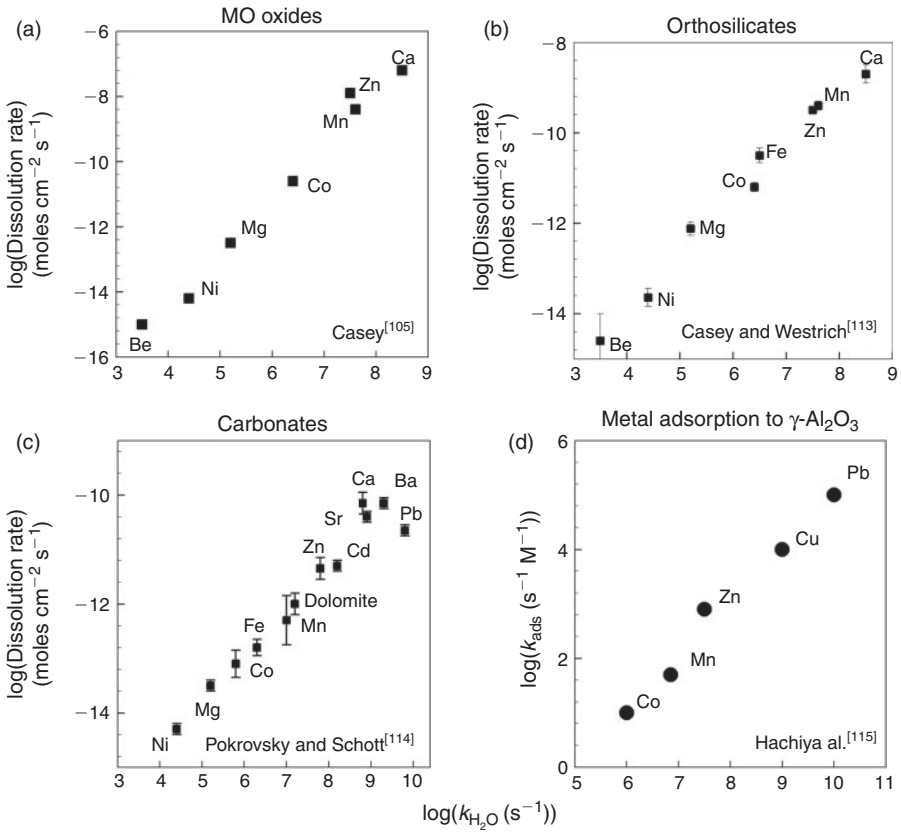

Fig. 4. Rates of several interfacial reactions at 298 K plotted against the pseudo-first-order rate coefficient for exchange of an inner-sphere bound water from around the corresponding metal in solution (k_{H_2O}) (adapted from Casey and Swaddle[62]). (a) The logarithms of dissolution rates at pH = 2 of simple metal-oxide minerals having the rocksalt-oxide structure, with labels referring to the stoichiometry of the mineral and the hydrated metal. The label '*Mg*', for example, refers both to dissolution rate of periclase (MgO) and the value of k_{H_2O} for $Mg(H_2O)_6^{2+}$. (b) Dissolution rates at pH = 2 of orthosilicate minerals having the olivine and phenakite structures. (c) A similar plot for dissolution rates of carbonate minerals having the calcite and aragonite structures,[114] with dissolution rates for $5 \leq pH \leq 8$ and $\Sigma CO_2 \leq 10^{-4}$ M. (d) The intrinsic rates of adsorption of different hydrated metals onto the surface of γ-Al_2O_3.[115] The reactivity trends are similar because all reactions reflect processes of ligand exchange around metals with similar coordination environments.

aluminium hydroxide ions to calibrate the accuracy of estimates for mineral surface functional groups on minerals like kaolinite and gibbsite. They found that their sampling was accurate only to within a factor of $\sim 10^2$ but that the rates of exchanges on minerals were so fast that they approach the rates found for ions like the alkali-metal ions; rates are near what is called the Smoluchowschi limit where diffusion of the reactants is the rate-controlling step. This simulation of simple ligand exchange at terminal functional groups, or ionic salts,[10] is an area that is ripe for rapid advancement in part because experimental data exist to distinguish failures from successes.

Removing a proton from a bound water accelerates rates

At terminal waters, *removal* of a proton from a cationic molecule is important because this reduces the overall charge of the aquo ion and the strength of the bond between the metal and any remaining oxygen. (Below cases are discussed where removal of a proton *reduces* rates.) The labilising role of protons in an aqueous geochemical reaction can be illustrated best by examining simple small molecules, where the Brønsted acid–base chemistry is unequivocal. First, let's look at what happens to one of the water-exchange reactions affecting a cationic monomer ion when a single proton is pulled off of a water bound to the complex. This question, restated, is how are ligand-exchange reaction rates affected by reduction of the overall charge of a cation?

$$[Fe(OH_2)_6]^{3+} + H_2O \leftrightarrow [FeOH(OH_2)_5]^{2+} + H_3O^+(aq) \quad (1)$$

The rates of ligand exchange of the first hydrolysis complex, $[FeOH(OH_2)_5]^{2+}$, is $\sim 10^2$ times more rapid than the rates of exchange around the more highly charged, fully protonated $[Fe(OH_2)_6]^{3+}$.[6,17,18] The increased reactivity is general for metal aquo ions – virtually all cations become more labile to ligand exchange as the overall molecular charge is reduced by deprotonation. Fig. 6 shows sets of reactions that illustrate this labilisation, from formation of oligomers to anation (adding an anion), to water exchange rates. These trends were established by using inert metals, like the low-spin d^6 Rh^{III} oxide complexes, where the rates are sufficiently slow to control.[19–39] The kinetics of reactions that are blisteringly fast in geochemical metals, like Fe^{III} and Al^{III}, are sufficiently slow to isolate the details with great confidence.

It is important to know the timescales. For most metals, protons also move around oxygens in the molecules in

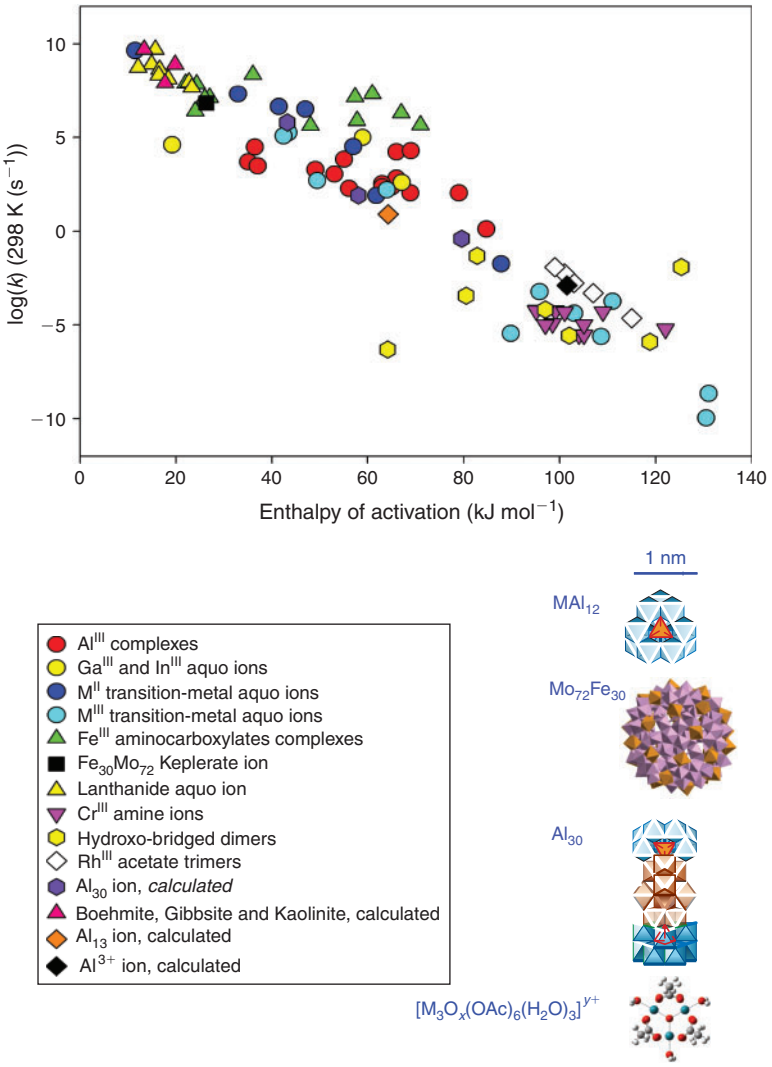

Fig. 5. A compilation of rates for replacement of a metal-bound water with one from the bulk for oxides having an enormous range of sizes (adapted from Ohlin et al.[116]). The abscissa is the corresponding activation enthalpy of the reaction. A strong correlation is evident because the entropies of activation tend to be near zero. Included in this plot are rates estimated for sites on aluminum-hydroxide minerals and nanometre-sized clusters.[11] The abbreviations are: $\mathbf{Al_{30}} = Al_2O_8Al_{28}(OH)_{56}(H_2O)_{26}]^{18+}$,[117–119] $MAl_{12} = [MO_4Al_{12}(OH)_{24}(H_2O)_{12}]^{7-8+}$, $Mo_{72}Fe_{30} = [Mo_{72}Fe_{30}O_{252}(CH_3COO)_{12}[Mo_2O_7(H_2O)]_2\ [H_2Mo_2O_8(H_2O)](H_2O)_{91}]$.[14,51] Rates tend to vary with metal charge, or metal-oxygen bond lengths. Large molecules (e.g. $Mo_{72}Fe_{30}$) tend to have lower average charge densities than small monomer ions (e.g. $Fe(OH_2)_6]^{3+}$), which accounts for the more rapid rates.

millisecond to submillisecond time scales, which is commonly more rapid than rates of oxygen-isotope exchanges. In other words, the net largest effect of the deprotonation reaction is usually through the average bond strength of the metal–oxygen bond. The proton visits all oxygens many times before an isotope-exchange event for metals that exchange in milliseconds and longer, like the inert metals discussed above. The exchanging moiety in these molecules is a bound water molecule because it is much easier to exchange an uncharged bulk water for a bound water than for a charged hydroxide ion where electrostatic energy must be additionally surmounted.

Conjugate acids and bases

Sometimes an incoming ligand can donate or remove a proton from the exchanging functional group as the exchange proceeds and accelerate the reaction. These are conjugate acid–base pathways. The cooperative role of a proton donation is well illustrated for a mineral setting by simple experiments where bound waters on complexes are created to have one- or two bound waters within distances close enough to share protons. Proton transfers during an exchange event have an immediate geochemical use because bound waters on mineral surfaces can be either isolated (*vicinal*) or paired (*geminal*) and these will have profoundly different pH dependencies to exchange.

In Fig. 7 are shown the variation in the logarithms of the rate coefficient for exchange of the bound waters on two nearly identical Rh^{III} bipyridine complexes[40]; they differ only by the proximity of an acidic proton to the exchanging water. In the molecule where there is no adjacent bound water, the rates drop precipitously as the pH approaches the pK_{a1} of the molecule.

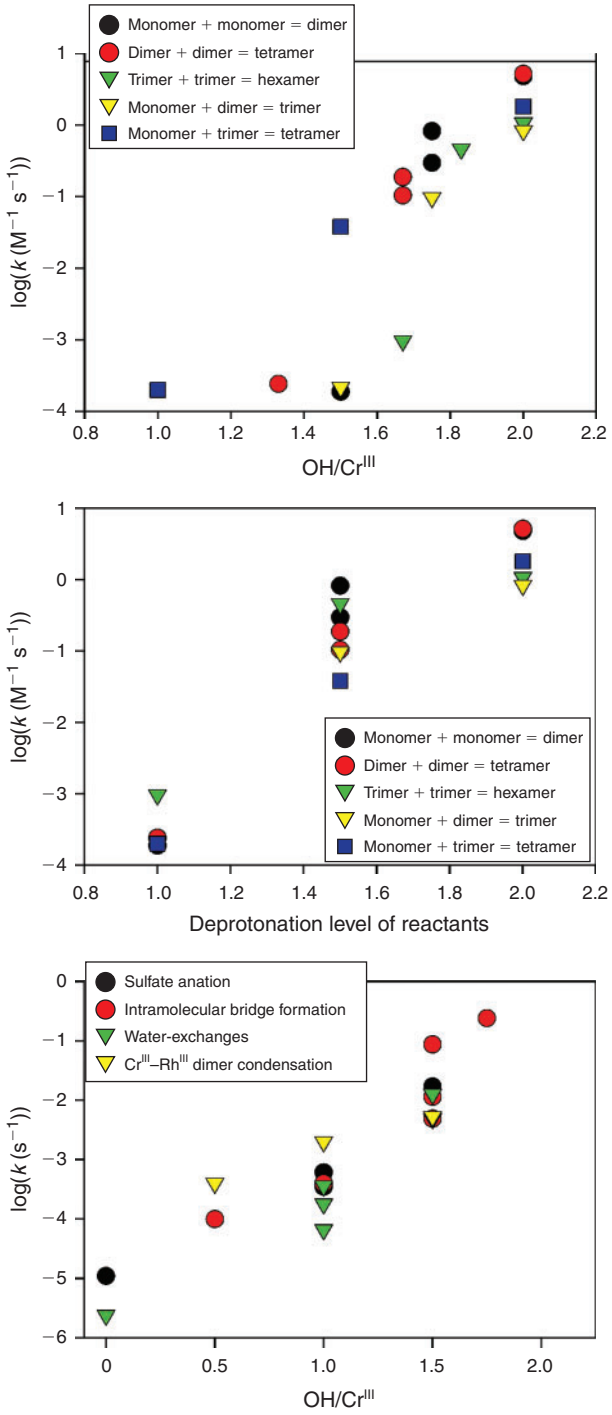

Fig. 6. A wide range of ligand-exchange reactions are labilised by deprotonation and the presence of structural hydroxide ions, which are stronger Lewis bases than bound waters. These include (top) hydrolytic condensation of Cr^{III} complexes into oligomers; (middle) condensation of inert-metal oligomers into higher-molecular weight oligomers; and (bottom) water-exchange rates, intermolecular condensation reactions and Cr^{III}–Rh^{III} dimer condensation and sulfate addition (see discussion and citation of original sources in Casey et al.[120]).

Here the bound water deprotonates to form a bound hydroxy group. The most suitable exchanging moiety in these reactions is a bulk water, and a bulk water most easily exchanges for a bound water, not a bound hydroxide, because there is no charge to compensate in exchanging a neutral water for another neutral water. So, when a bound water is deprotonated, the rates drop because the concentration of the exchangable moiety, the bound water, decreases and it is harder to remove a bound hydroxide ion from a cationic metal than a neutral bound water. (The situation can be different at very high pH where a dissolved hydroxide ion exchanges for a bound hydroxide, but at near-neutral pH conditions, there are so few bulk hydroxide ions that the rates of exchange by this pathway are slow.)

Other chemistry altogether occurs when there are two bound waters that lie close enough to transfer acidic protons back and forth as $pH > pK_{a1}$. When the first bound water in this complex is deprotonated, the charge of the complex decreases so that the metal–oxygen bond strengths are weaker, but it is now possible for the remaining bound water molecule to donate a proton to the nearby bound hydroxy group. When the pH approaches the pK_{a1} of the molecule, the rates of isotopic exchange soar by almost $\sim 10^4$ (Fig. 7) and peak when $pK_{a2} > pH > pK_{a1}$. It is only when both bound-water functional groups are deprotonated at $pH > pK_{a2}$ that the rates decline with pH, as they did for the molecule with a single bound water.

Bridging oxygens

Whereas the rate of exchange of bound waters, or virtually any terminal ligand with $^1\eta$ bonding, seems to be somewhat predictable in water, the rates of exchange of the bridging oxygens are exquisitely sensitive to details of the structure and bonding. Pioneering work on small molecules was performed by scientists such as Murmann, Spiccia, Springborg and Swaddle, who constructed hydroxy-bridged molecules out of inert metals such as Cr^{III}, Co^{III}, Rh^{III} and Ir^{III}, or even aluminosilicate oligomers, and then worked out the rate laws for hydrolytic reactions that cleave and form the molecules.[2,8,20,23–35,41–48]

Data for these small molecules that can really help us understand the role that protons play in labilising reactions like isotope exchanges and dissociations. In Table 2, for example, equilibrium constants are shown for Cr^{III}-oxide clusters of varying sizes (see the works of Spiccia[19,20] and Springborg[48]). For anions, the polyoxometalate community[49–59] has long worked to establish reaction pathways in nanometre-size ions, usually anions of Group V and VI metals.

In general, knowledge about the reactivity of bridging oxygens varies inversely with their coordination number. Usually more highly coordinated oxygens (e.g. μ_3-O(H), μ_4-O, μ_6-O) react more slowly than lower-coordinated oxygens, such as μ_2-OH bridges, although some exceptions can be found. The differences between different oxygens can be quite profound. Murmann and Shelton[60] and Rogers et al.,[61] for example, studied oxygen-isotope exchange in the molybdenum(V) cluster $(H_2O)_3(\eta\text{-O})Mo(\mu_2\text{-O})_2Mo(\eta\text{-O})(OH_2)_3^{2+}$ and found that the characteristic time for exchange of the μ_2-O groups with bulk solution is over 100 h at 40 °C, but the singly coordinated oxo groups (η-O) exchange within minutes even at 0 °C and the η-OH_2 sites exchange in a few milliseconds or less at 25 °C. Similarly, the oxygens in silicate clusters react in sub-second time scales in small monomers, dimers and trimers, but are very slow or inert in the large, more rigid, silicate octamer.[41,42,62–76]

Protonation of oxygens is key to understanding the pH variation of the rates but the location of the proton and the charge of the molecule controls its effect. A key path for hydrolysis and isotope-exchange reactions in small oligomers involves protonating the μ_2-OH bridges to form μ_2-OH_2, which are very weak. Even as a transient bridge, they lend themselves to facile exchange for a bulk water molecule or complete

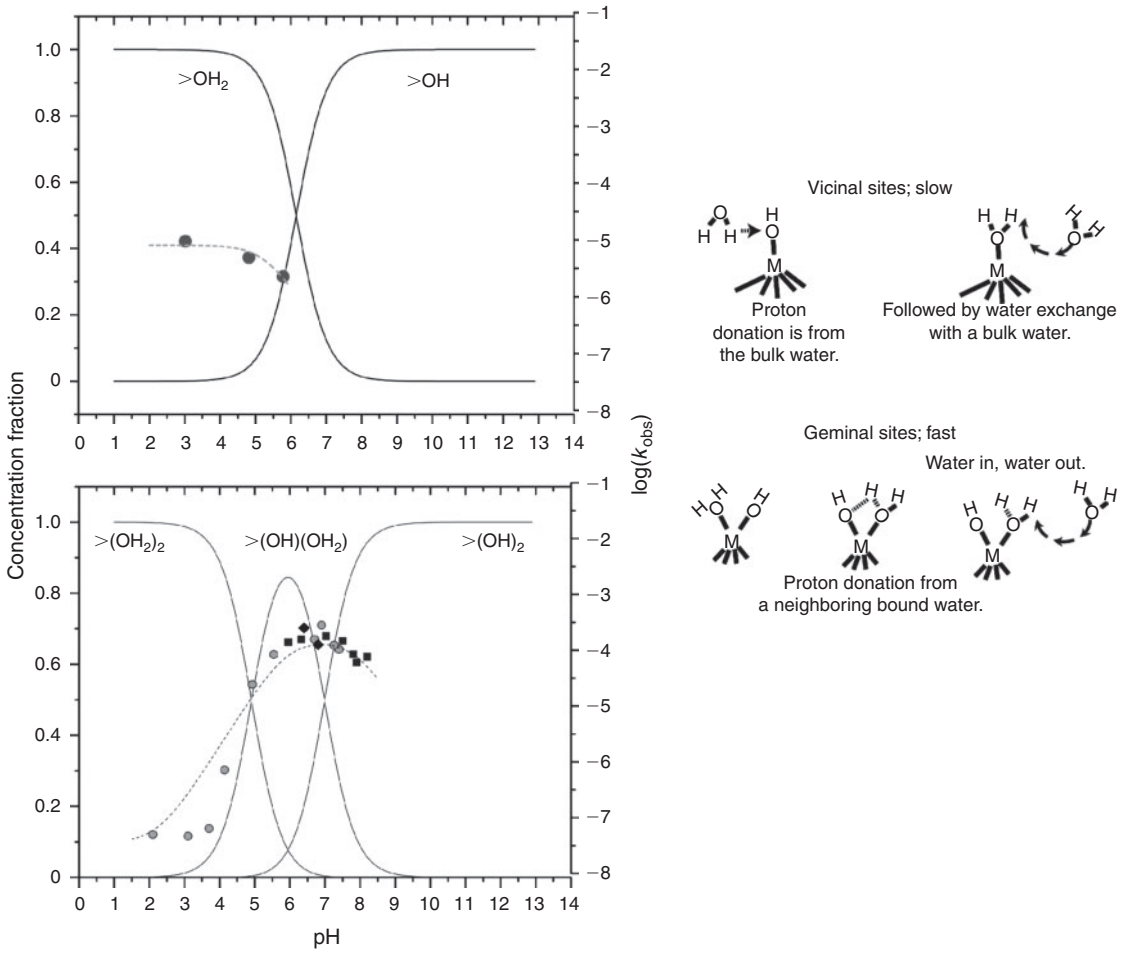

Fig. 7. The rates of exchange of terminal ligands are easiest when they can be converted to an exchangeable water molecule and this depends on the local site structure.[40] On the left are the pH dependencies for oxygen-isotope exchange into two molecules that differ only in the proximity of a tranferable proton. In the top case, the rates of isotopic exchange drop precipitously when pH ≈ pK_{a1}. At the bottom rates increase by orders of magnitude when pH–pK_{a1} because charge is reduced and the adjacent water can donate a proton to facilitate the exchange with a bulk water. The reaction is illustrated in cartoons on the right.

Table 2. Deprotonation constants of terminal water molecules in Cr^{III} complexes as a function of the number of metals in the complex at $I = 1.0$ m[34,38,106]

Stoichiometry		pK_{a1}	pK_{a2}	pK_{a3}
$[Cr(H_2O)_6]^{3+}$	Monomer	4.29	6.1	
$[Cr_2(OH)_2]^{4+}$	Dimer	3.68	6.04	
$[Cr_3(OH)_3]^{5+}$	Trimer	4.35	5.63	6.0
$[Cr_4(OH)_6]^{6+}$	Tetramer	2.55	5.08	

Table 3. Deprotonation constants of μ_2-OH ligands in bridged Cr^{III} ammine dimers as a function of different ligands at the non-bridging sites[48]

Note that the μ_2-OH_2 bridge is a much stronger Brønsted acid than the η-OH_2

Stoichiometry	pK_a
Singly bridged dimers	
cis-$[(NH_3)_5Cr(\mu_2\text{-}OH)Cr(NH_3)(enH)]^{6+}$	6.36
$[(NH_3)_5Cr(\mu_2\text{-}OH)Cr(NH_3)_5]^{5+}$	7.63
trans-$[(NH_3)_5Cr(\mu_2\text{-}OH)Cr(NH_3)_4(OH)\ ]^{4+}$	~9
cis-$[(NH_3)_5Cr(\mu_2\text{-}OH)Cr(NH_3)_4(OH)\ ]^{4+}$	>16
cis-$[(NH_3)_5Cr(\mu_2\text{-}OH)Cr(NH_3)_4(NCS)\ ]^{4+}$	10.6
trans-$[(NH_3)_5Cr(\mu_2\text{-}OH)Cr(NH_3)_4Cl]^{4+}$	11.4
cis-$[(NH_3)_5Cr(\mu_2\text{-}OH)Cr(NH_3)_4F]^{4+}$	13.4
Doubly bridged dimers	
$(NH_3)_4Cr(\mu_2\text{-}OH)_2Cr(NH_3)_4^{4+}$	~12

dissociation of the molecule. An isotopically distinct water leaves the oligomer and is replaced by a bulk water that either deprotonates if the molecule is to remain stable, or dissociates at the bridging water as another water molecule adds to the outgoing metal.

The relative fraction of μ_2-OH_2 and μ_2-OH is controlled by the solution pH as this acid–base chemistry introduces a distinct pH dependence to an otherwise slow and pH-independent reaction rate. The μ_2-OH_2 group is a much stronger Brønsted acid than the η-OH_2 sites in hydroxo-complexes (compare Tables 2 and 3), which means that it is experimentally difficult to determine a protonation constant at these key oxygens, even for molecules for which the structure is unequivocal. (Here is one disadvantage of using only small molecules to infer

geochemical reaction pathways – small molecules can't hold together like the large, nanometre-sized structures described in the next section).

However, from these studies of aqueous complexes it is clear that the Brønsted properties are very sensitive to small changes in structure and to ligand substitutions. For example, the protonation constant for μ_2-OH bridges in the *trans*-$[(NH_3)_5Cr(\mu_2\text{-}OH)Cr(NH_3)_4(OH)]^{4+}$ molecule is $\sim 10^7$ smaller than for the *cis*-$[(NH_3)_5Cr(\mu_2\text{-}OH)Cr(NH_3)_4(OH)]^{4+}$ molecule, although these molecules differ only in the position of the η-OH^- site (Table 3). The effects that ligand substitutions have on the dissociation rate can be *direct* if the ligands weaken bonds between the metal and the bridging hydroxy molecule. The influence is *indirect* if the ligand changes the Brønsted properties of the hydroxy bridges so that they become more (or less) susceptible to protonation and hence proton-promoted cleavage. For mineral surfaces, this means that anion adsorption may accelerate dissolution because the reduced surface charge allows for more protons to adsorb. Ligand- and proton-promoted dissolution processes are usually treated as independent by aqueous chemists, but they may be intimately linked.

Activation energies for dissociation are also measurably reduced by protonation. For example, the enthalpy of activation for dissociating the $[(NH_3)_5Co(\mu_2\text{-}OH)Co(NH_3)_5]^{5+}$ dimer is 84 kJ mol^{-1} for a pH-independent pathway, but is reduced to less than 50 kJ mol^{-1} for reaction by the proton-promoted pathway (see Springborg[48] and Casey and Sposito[77]). This proton-promoted pathway for breaking a bond is most relevant for environmental chemists because they usually conduct their dissolution and desorption studies in acid solutions and use pH as a key variable, which confounds the simple interpretation of activation energies.[77] Protons *catalyse* bond cleavage if they are recycled after the reaction. *Induced* reactions are more common in geochemistry because the hydrated monomers (e.g. $[Co(H_2O)_6]^{3+}$) released by dissociation of a dimer (or dissolution of an oxide mineral) are weaker Brønsted acids than the μ_2-OH_2 bridge. Once the oligomer has dissociated, the labilising protons are retained by the monomers in their hydration-sphere waters to undergo normal exchange – there is no catalysis. The contribution of protonation enthalpy to the activation energy maps directly to dissolution kinetics of oxide minerals, where the Brønsted reactions are measured as surface charge.[77] Thus it should not be surprising that the experimental activation parameters in a typical soil or geochemical study, such as dissolution of a mineral, vary with pH. The contribution of enthalpy from Brønsted acid–base reactions is merely becoming evident in the lumped experimental parameter.

Chelating ligands

Most metals important to aqueous environmental chemistry are high in the periodic table and thus bond well to hard Lewis acids like oxygen. First-row transition metals can also bond to reduced nitrogens in amine functional groups or to reduced sulfurs in thiol moieties. The stability of the ligand to complex the metal can be greatly enhanced by organising the bonding functional groups into a chain, which eliminates the entropy of adding each monomeric ligand to a binding site. There are many good examples, but the ligation of ammonia to Cu^{II} provides a good quick illustration. The logarithm of the equilibrium constant to bond four NH_3 ligands to Cu^{II} is $\log \beta_4 = 13.0$. If two of the bonding nitrogens are linked with a carbon backbone (making ethylenediamine) the equivalent equilibrium constant to bond Cu^{II} with four nitrogens is $\log \beta_2 = 19.6$ and if all four nitrogens are linked together in a single molecule, the equilibrium constant is $\log K = 20.1$. Thus, the chelated metal is much more stable than the same metal bonded to monomeric ligands .

When one speaks of the kinetics of chelation reactions there are really two separate reactions of concern, at least to a first approximation. First there is the labilising effect of the stable chelate on other ligands in the molecule. For example, addition of oxalate chelate ($[C_2O_4]^{2-}$) to Al^{III} causes the remaining bound waters in the $[AlC_2O_4(OH_2)_4]^+$ to increase their rates of ligand exchange with bulk waters substantially . The oxalate here is a 'spectator' ligand and their influence on the reaction kinetics is predictable, at least if the ligands aren't so large as to fully encapsulate the metal, using the same reactivity trends described above for monomeric ligands. For bound waters, the largest effect of the spectator ligand arises from the reduction of complex charge and the corresponding reduction in metal–oxygen bond strength in adjacent ligands. The effect needn't be ionic – addition of a bonded amine ligand to a metal can labilise bonded waters to increase their rates of exchange with the bulk waters simply by donating charge to the metal covalently. The enhanced labilities are almost invariably accompanied by lengthening of the key M–OH_2 bond length and the large aminocarboxylate ligands like EDTA provide wonderful examples. Rates of water exchange in these complexes of Fe^{III} are on the timescale of $\sim 10^7$ s^{-1},[78–80] many orders of magnitude faster than the $[Fe(OH_2)_6]^{3+}$ ion (~ 160 s^{-1}[6,17]). Some of these ligands even increase the coordination number of Fe^{III} from six to seven, further weakening the remaining M–O bond strength to water and enhancing the rates of substitution at that site. Obviously packing of atoms around the metal disrupts hydrogen bonding in the solvation sphere, which modifies the mechanism of exchange, but these too are understood. Mechanism in this sense means the extent to which the incoming exchanging bulk water forces the coordination sphere to distort.

The second type of reaction concerning chelating organic ligands is the rate at which the molecule fully forms its chelated structure by successive ligand exchanges. For a multidentate ligand like EDTA there are obviously many ligand exchanges that can affect a metal and the reaction pathways are complicated (see Margerum et al.,[1] for a dated but still useful review). The mechanism of chelation are successive attachments of the ligands, closing rings of atoms with bonding to the metal. The kinetics of these reactions are difficult to detail for such multidentate ligands because so many processes must be followed – for each bonded ligand and for the large molecule as a whole. However, the pathways for these reactions have been well studied in simpler systems, such as bidentate chelates, and they are discussed below to illustrate the key chemistry, again with the caveat that this presentation is in no way complete.

For multidentate chelating ligands, these sometimes have arms that could be bonded, but aren't. EDTA has four acetate groups and two ternary amine groups that could bond to a metal, making six in total. A *pendant arm*, for example, might be an unbonded acetic acid moiety on the EDTA that flops around in solution whereas the other three acetates are firmly bound to Fe^{III}, making a complex like $[Fe(EDTA)OH_2]^-$(aq). The bound water will be quite labile for reasons discussed in the preceding paragraph and occupies the single octahedral site around the metal that is not taken up by functional groups from the chelate. This stoichiometry is only possible because one of the four

acetates in the $EDTA^{4-}$ ligand is unbonded, or pendant (Scheme 1, adapted from Maigut et al.[79]).

To a first approximation, ligation for a multidentate ligand involves two steps: (i) initial ligand exchange to add a bonded atom and (ii) ring closures as the other ligands attach stepwise. One of these two steps usually controls the overall process and small five-atom chelate rings are usually most stable. This chemistry is well probed in simple systems and one of the most detailed is the formation of diol complexes of boron. Boron (B^{III}) is special among metals because it, like Al^{III}, changes coordination number easily in aqueous solution.

The $[B(OH)_3]^0$ molecule is trigonal and the borate ion, $[B(OH)_4]^-$ is tetrahedral; thus boric acid is an oxyacid that doesn't just take up and lose protons, like $[H_2PO_4]^-$ and virtually all other oxyacids, but by adding a hydroxide ion to the inner-coordination sphere of $[B(OH)_3]^0$. This change in coordination has been exploited to understand better the general processes of chelation by various substituted diols, both aliphatic and aromatic.[81–87] The detail available from these studies is superb because the change in boron coordination yields a distinct ^{11}B NMR signal and because the authors can modify both the ligand diol and metal complex systematically for stopped-flow kinetic studies.

This reaction has two steps: (i) displacement of a bonded hydroxide by an incoming oxygen on the chelating diol (e.g. catechol) and (ii) addition of another atom to the B^{III} to make the four-coordinated complex (Scheme 2). For most geochemical metals, this step would displace an existing bound water but conserve the overall coordination number of the metal – it would not be a ligand addition but a ligand exchange. Early work argued that the rate-controlling step was collapse of the second bonding oxygen in the diol (e.g. catechol), thereby increasing the coordination number of B^{III}. Evidence for this conclusion was found in the strong correlation of rates with Brønsted acidities of the incoming bidentate ligand (a diol), clearly indicating that proton transfer, which is evidently important in Scheme 2, was involved in the rate-controlling step. The rates of complexation increased when the ligand protons were easily displaced and added to an outgoing hydroxy group as a water molecule.

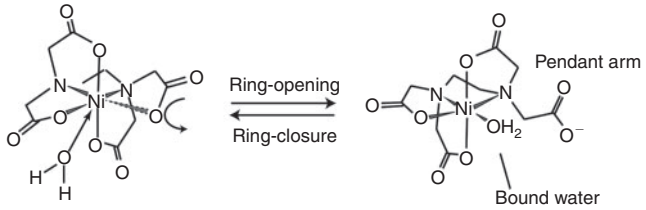

Scheme 1.

However, a revision was later required through experiments with boron complexes that could be structured such that the metal was forced to exist in either tetrahedral or trigonal B^{III}, but not switch coordinations. In these cases it was concluded that the first step, ligand addition, actually controlled the reaction rate and that once this attack was successfully accomplished, the ring collapse was fast, forming the chelated complex.

For environmental chemists, among the most important natural chelating ligands that have a defined structure are the siderophores, which are used to sequester nutrient iron in soil solutions where the solubility of ferric hydroxide solid is so vanishingly small. The architecture of these molecules is somewhat similar to EDTA in that six ligands are conjoined by a carbon backbone to completely encapsulate Fe^{III}. There are two particularly interesting classes of siderophores, the tris-hydroxamate siderophores and the tris-catecholate siderophores (others exist[88]). The catecholates have three sets of bidentate catechols, with coupled functional groups similar to the reaction shown in Scheme 2 for boron reactions. The hydroxamates are also three sets of bidentate ligands, but in this case they are coupled –C=O and –N–OH functionalities. The molecules themselves are often large structures and these are also used as drug candidates for diseases of iron overload, such as Thallasemia. The most common being desferrioxamine, in a commercial form known as Desferal.

The kinetics of ring-formation in desferrioxamine around Fe^{III} have been determined by experiment[88] and are consistent with the rate-controlling step being a leaving water molecule bound to the Fe^{III} metal. For example, the second-order rate constant for chelation by desferrioxamine to $[Fe(OH_2)_6]^{3+}$ is 0.2 $M^{-1}\,s^{-1}$ but increases by a factor of $\sim 10^3$ when the pH is raised so that the first hydrolysis product, $[FeOH(OH_2)_6]^{2+}$, dominates, as one expects if the elimination of a bound water were important to ring closure. Subsequent ring-closure steps proceed at approximately the same rates, which indicate that these reactions are not limited by water-loss rates. The siderophores are effective at transporting Fe^{III} because all six coordination sites around the metal are bonded to functional

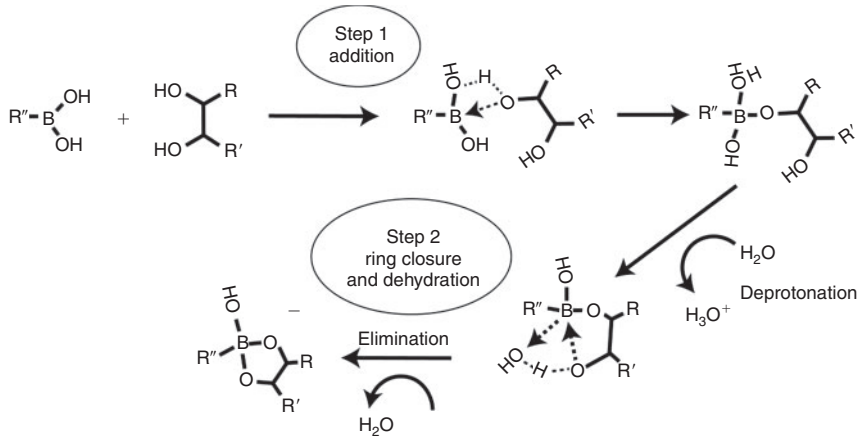

Scheme 2.

groups in the chelate. The stepwise rate for the bidentate models of a trisbidentate catecholate siderophore (here, TIRON = 1,2-dihydroxy-3,5-benzenesulfate) are typical. Here one can start with the hydrolysed iron[88]:

$$[FeOH(OH_2)_6]^{2+} + LH_x \rightarrow [FeL(OH_2)_4]^{(3-x)+} + (x-1)H^+; \quad k_1 = 1.7 \times 10^3$$

$$[FeL(OH_2)_4]^{(3-x)+} + LH_x \rightarrow [FeL_2(OH_2)_2]^{(3-2x)+} + xH^+; \quad k_2 = 3.2 \times 10^3$$

$$[FeL_2(OH_2)_2]^{2+} + LH_x \rightarrow [FeL_3]^{(3-3x)+} + xH^+; \; k_3 = 7.7 \times 10^3$$

Kinetics in the full encapsulating siderophore may be different, but this example shows that chelation steps are not particularly accelerated by the pre-existence of a bidentate chelate in the complex. The Lewis basicity of the first chelate is not sufficient to accelerate subsequent chelation steps – the rates, to a first approximation, are the same for each step. Reversal of the chelation reaction commonly involves a reduction of the Fe^{III} to the more labile Fe^{II}, for which the trischelates have much lower affinity – this is reductive dissolution when applied to minerals but is reductive dissociation for chelate complexes.

In summary, there are clear messages for environmental scientists from these superbly detailed studies. First, molecular details of the activated complex and rate-controlling steps are hotly debated, even for these well probed B^{III} reactions where donors and acceptors can be adjusted systematically. There is no wisdom to be gained by speculating about rate-controlling steps at the molecular scale for geochemical reactions without marshalling a similar armoury of such data first. The only possible justification for such speculation is to establish large-scale predictions for entire classes of molecules that differ systematically from one another. Thus, for example, knowing about the kinetics of reactions in hexadentate aminocarboxylate ligands might be useful for predicting the reactivities of tetradentate or pentadentate chelates.

Second, much more important than the molecular details are the causes of slow kinetics in natural waters, which aren't controlled by such things as pendant arms and changes in coordination. Experimentally, ligand-exchange and ligand-addition reactions involving chelated metal complexes are fast, even reactions such as those in Scheme 2 where the metal coordination changes. Chelation at mineral surface atoms will, of course, be slower because of the steric hindrances, but the time scales are, at most, minutes to a couple of hours or there are other reactions involved. Steric hindrances are also expected to affect rates in large natural polyelectrolyte molecules like humic acids. Usually if complexation reactions are slow, it is because there is either a slow, unknown solute-transport step that is limiting the reaction rate, or the activities of the free metal and free ligands are small because of competing fast reactions.[89] This latter condition is worth more discussing further.

Reactions that are inherently fast in the laboratory are often grindingly slow in the field. The reasons aren't exotic – rate laws for polydentate complexation are usually expressed in terms of uncomplexed (*free*) metals and ligands, which can be kept high in experimental solutions but are never so in natural waters. Natural waters have an ensemble of metals and ligands that compete with one another and a good rule of thumb is that weak bonds form quickly and strong bonds form slowly.

In a multicomponent solution like seawater, *free* metals or *free* ligands bond quickly to one another and, once bonded, are unavailable for further chelation. Thus, complexation of any metal or ligand that is added to a natural water experiences a cascade of stepwise reactions. Weak ligands bond quickly, but are then displaced by stronger ligands at rates that are proportional to the small free concentration. Polydentate metal complexes do a poor job of associatively affecting other such complexes. Similarly, strong multidentate ligands bond to abundant metals and are slowly displaced by metals that form stronger bonds to the functional groups in the chelating ligand. Thus, for example, Ca^{II} is abundant in seawater and scavenges added EDTA immediately. Bonding in the EDTA is through the acetate oxygens and is relatively weak. With time, the Ca^{II} is displaced by transition metals like Fe^{II} or Ni^{II}, which form even stronger bonds to EDTA by the oxygens and the amine nitrogens, but exist at much lower concentrations in natural waters. The final thermodynamic state is reached by a slow cascade of complexation, release and re-complexation reactions.

These slow kinetics have enormous implications for the degradation of pollutants on the human lifescale. EDTA, our example chelating agent, is a pollutant that degrades photolytically when complexed to a metal that allows one-electron oxidations, like Fe^{III}. Photodegradation of pollutant EDTA is diurnal and requires the Fe–EDTA complex, but the ligand is partitioned among many metals in natural waters, most of which are photolytically inert.[90,91]

A final caveat

Above is presented an essential ionic view of these reactions, which is wrong in detail and often very wrong. One case has already been touched upon, where the labilities of bound ligands on metals within a single Group decrease (e.g. Co^{III}, Rh^{III} and Ir^{III}), which requires a more sophisticated understanding of bonding than is provided here as metal charge densities. Similarly the presence of multiple-bond order in oxo complexes, such as $[UO_2]^{2-}$ or $[WO_4]^{2-}$, is a quantum-mechanical phenomenon. Even the lability of Ni^{II} complexes upon addition of additional NH_3 ligands can illustrate the point well (Table 4). The rates of exchange of a bound water increase by factors of 10–100 upon addition of each additional ammonia to the inner coordination sphere, forming a series of $[Ni(NH_3)_x(OH_2)_{6-x}]^{2+}$ complexes of identical overall charge. The bound waters are labilised because of charge donation from the nitrogen to the metal that weakens bonds to the inner-sphere water. Such an effect is inherently covalent and requires a better understanding of bonding than has been imparted above by emphasising only charge densities, but there exist superb reviews.[7]

Larger oxide structures

Small molecules allow superb resolution of the kinetic processes at work, but provide limited insights into the oxide structures that concern geochemists and soil chemists, like the nanometre-size structures on mineral growth and dissolution features. However, work on isotope-exchange reactions in nanometre-sized clusters over the last decade has provided guidance to understanding reactions at these larger structures. What scientists have learned is that the pathways for ligand- or isotope-exchange reactions involve metastable equilibria and that there exist a few sets of rules to understand how these form and react. These are discussed in the next section.

Table 4. Rate coefficients (k_{298}) for exchange of a single water molecule from around Ni^{II}–ligand complexes[1,107–112]

Complex	k_{298} (s^{-1})	Complex	k_{298} (s^{-1})
$[Ni(H_2O)_6]^{2+}$ [A]	0.32×10^5	$[Ni(NH_3)(H_2O)_5]^{2+}$ [A]	2.5×10^5
$[Ni(NH_3)_2(H_2O)_4]^{2+}$ [A]	6.1×10^5	$[Ni(NH_3)_3(H_2O)_3]^{2+}$ [A]	$25. \times 10^5$
$[Ni(en)(H_2O)_5]^{2+}$ [B]	4.4×10^5	$[Ni(dien)(H_2O)_3]^{2+}$ [B]	$18. \times 10^5$
$[Ni(trien)(H_2O)_2]^{2+}$ [B]	29×10^5	$[Ni(en)_2(H_2O)_2]^{2+}$ [B]	$54. \times 10^5$
$[Ni(bpy)(H_2O)_4]^{2+}$ [C]	0.49×10^5	$[Ni(bpy)_2(H_2O)_2]^{2+}$ [C]	0.66×10^5
$[Ni(tpy)(H_2O)_3]^{2+}$ [C]	0.52×10^5		
$[Ni(ida)(H_2O)_3]^{2+}$ [D]	2.4×10^5	$[Ni(H_2O)(edta)]^{2-}$ [D]	7×10^5
$[Ni(H_2O)_5Cl]^{+}$ [E]	1.5×10^5	$[Ni(H_2O)_3(NCS)]^{3-}$ [E]	11×10^5
$[Ni(2,3,2\text{-tet})(H_2O)_2]^{2+}$ [F]	40×10^5	$[Ni((12[ane]N_4)(H_2O)_2]^{2+}$ [F]	200×10^5

[A]Ammonia.
[B]Tertiary amines.
[C]Pyridines.
[D]Carboxylates.
[E]Inorganic ligands.
[F]Macrocycles.

Some macroscopic reactivity trends

As discussed earlier, the dissolution of an oxide mineral in water proceeds by a series of ligand-exchange reactions that replace bridging oxygens with terminal waters until a solvated ion is released. One should be able to explain the broad reactivity trends as long as there are no redox steps that might affect reactivities. It shouldn't be surprising that the rates of dissolution of fully protonated oxides scale like the inherent reactivity of the constituent metals to ligand exchange (Fig. 2). There are, however, some unique features of dissolution of a mineral. These can only be understood by examining the pathways for oxygen-isotope exchanges and ligand exchanges in nanometre-size oxide ions. These include:

(1) Reactivities often express *average* composition. For dense, nonporous minerals without a strongly anisotropic or polymerised structure, the dissolution rates tend to reflect the average mineral composition, not the reactivities of individual metal–oxygen sites. One can obviously make a structure with functional groups that act independently. For example, it is possible to sandwich a brucite-like layer between two lacunary tungstate polyoxometalate ions. In this case, functional groups on the sandwiched metal–hydroxide layer remain largely unaffected by the confining tungstate ligands. The sandwiched moiety is so profoundly distinct in structure and bonding compared to the ligating tungstate ions that it reacts as a separate structural component. However, what is most striking is the opposite observation – in cases like the orthosilicate minerals and simple oxide solids, where the structure is not heterogeneous, the reactivity is an expression of the *average* composition. This result is stunning.

Consider the examples shown in Fig. 8. The pure compounds, here orthosilicate minerals like liebenbergite (Ni_2SiO_4), exhibit exactly the reactivity trends one expects from ligand exchange for the first-row transition metal ions, like $[Ni(OH_2)_6]^{2+}$ – there is perfect correlation between the rates of dissolution of the solid and the rates of exchange of bound waters around the corresponding hydrated ion, as was seen in Fig. 3. What is important is the similar trend in reactivities, not the absolute values, which differ enormously.

However, if one makes an orthosilicate mineral that has the stoichiometry of $CaMgSiO_4$ (monticellite) and examines the dissolution kinetics, one doesn't see the Ca^{II} removed quickly from the exposed surface and the Mg^{II} reacting more slowly. Instead one sees a dissolution rate that is the weighted sum of contributions from each metal (Fig. 8).

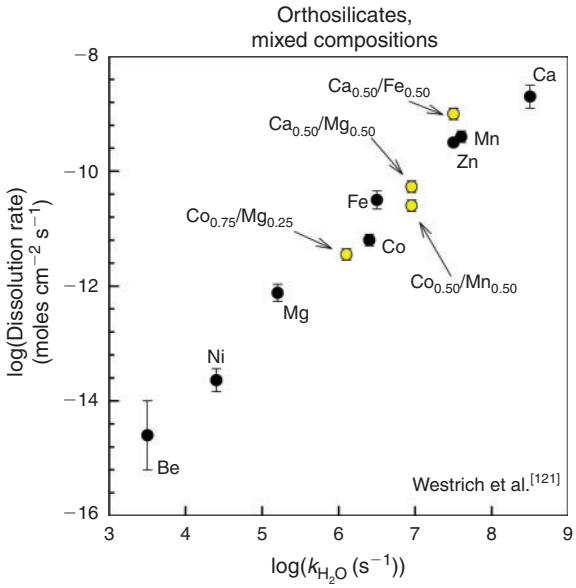

Fig. 8. Dissolution rates of orthosilicate and oxide minerals exhibit an averaging of reactivity according to composition. Here, orthosilicate minerals with intermediate compositions (yellow) exhibit a dissolution rate that is the weighted sum of rates for each end member.[121] One doesn't react away the most labile metal and leave the resistant metal to dissolve at its slow rate from the surface; an intermediate composition yields and intermediate rate.

(2) Dissolution rates are broadly amphoteric, meaning that the rates increase when the surface is a proton donor and when the surface is a proton acceptor. Practically, this means that rates go up at low pH and high pH conditions, sometimes with a region at intermediate pH conditions where the rates are nearly independent of pH. The exact location of this minimum depends upon the average proton affinity of the surface or the molecule. These broad amphoteric reactivity trends are commonly found when any oxide reacts with water. Hydrolysis of esters, isotope-exchange reactions in sugars etc all exhibit a broad amphoteric chemistry.

(3) Counterions sometimes affect oxide dissolution rates to a measurable extent. Much was made of this effect in transition-state models of mineral hydrolysis where it was assumed that the counterions are somehow directing electron-pair bonds to a transition state.[92] The truth is much more prosaic and derives from studies of isotope exchanges and electron exchanges (e.g. Czap et al.[93]), in oligomers and nanometre-sized oxide ions. As we discuss below, isotope-exchange into a structural bridge in these molecules requires formation of an intermediate structural form with lowered symmetry and accessible oxygens. Because charge separation is required in forming the intermediate, counterions can affect the rates by the extent of intermediate formation.

Oxygen-isotope exchanges in nanometre-size structures

Even an ion with 40–100 atoms already exhibits the same general reactivity trends discovered above from mineral-dissolution studies. Oxygen-isotope exchanges proceed by complicated pathways that would be nearly impossible to arrive at by visual examination of the structure, guessing the reaction coordinate and calculating a barrier height based on the guessed coordinate. In the two examples described below, the ions are the same size, or larger than, the cluster models used to simulate glass and mineral dissolution or the kink sites in step-flow models of the mineral surface.

Oxygen-isotope exchanges in polyoxoaluminum cations

The first set of molecules is the MAl_{12} series of aluminium ions that have the ε-Keggin structure (Fig. 1, top) and the stoichiometry: $[MO_4Al_{12}(OH)_{24}(H_2O)_{12}]^{7-8+}$, where the central metal is $M = Al^{III}$, Ga^{III} or Ge^{IV}. The structure consists of four planar trimeric $Al_3(OH)_6$ groups that are linked to the central M site by four inert μ_4-O. These molecules have a water molecule bound to each of the external aluminium atoms (twelve in total) and two distinct sets of twelve μ_2-OH correspond to the shared edges of $Al(O)_6$ octahedra. Unchanging isotopic signals in these μ_4-O sites indicate that the molecule remains intact as the isotope-exchange reactions affect other sites. These four μ_4-O only lose their isotopic uniqueness if the molecule completely dissociates and then reforms, so one can state with confidence that the μ_2-OH are undergoing isotopic exchange with the solution from an intact molecule. Unsurprisingly, rates of isotopic exchange of the bound waters are nearly identical across the series ($k^{298} \sim 10^3\ s^{-1}$) and the pH dependencies are simple, consistent with our discussion above – exchange of terminal water molecules are not sensitive to minor details of the structure but reflect a reduced charge density on the Al^{III} that weakens the Al–O bond. These rates are insensitive to isovalent substitutions into the 'M' site. Even an increase in charge upon Ge^{IV} substitution for Al^{III} has only a very small effect because the net difference in ion valence (+8 *v.* +7) is distributed across a structure with a diameter of ~1 nm. The difference in average charge density is small.

In contrast, rates of oxygen-isotopic substitution into μ_2-OH are enormously sensitive to the cation in the inert core, and span a range larger than $\sim 10^7$ in the order: $GeAl_{12} > Al_{13} > GaAl_{12}$. Thus one is left with an apparent paradox – rates of exchanges into some bridging oxygens, the μ_2-OH, are enormously sensitive to a metal substituted in the inert core, which is far removed from the reaction.

The reason isotope exchanges into the twelve μ_2-OH are sensitive to structure is because the molecule equilibrates with a metastable form that is required for the isotopic substitution to occur.[94] The stable condensed form of the ε-Keggin structure, with T_d symmetry, probably allows no steady oxygen-isotope exchanges. For isotopic exchange, the T_d form must partly dissociate to create a loose, dimer-like cap. This cap then dissociates further at one of the μ_2-OH to form an μ_2-H_3O_2 bridge that allows facile exchange of the bound water with an isotopically normal water from the bulk.[94,95] Replacement of a water in the μ_2-O_2H_3 bridge probably proceeds in millisecond time scales, like replacement of a bound η-OH_2 in the stable molecule.

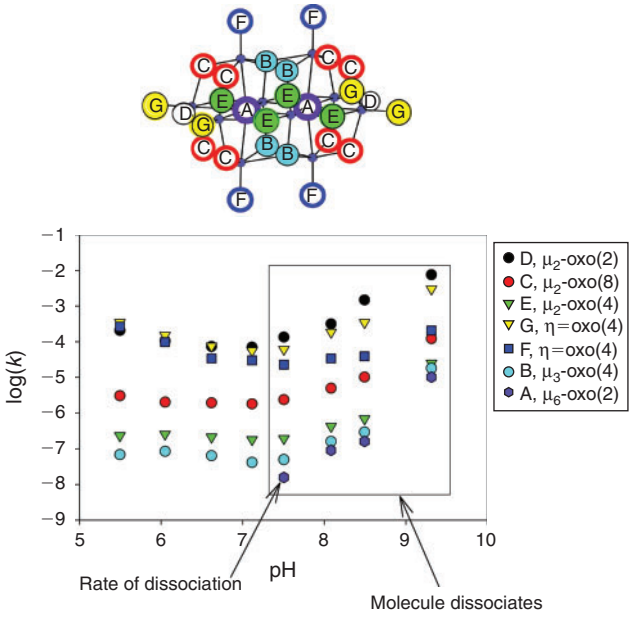

Fig. 9. The rates of steady oxygen-isotope exchanges for all seven structural oxygens in the $[H_xNb_{10}O_{28}]^{(6-x)-}$ ion, with the data coloured to identify each structural oxygen. As one can see, the rates span ~10^4 but all oxygen sites exhibit the same pH dependence, indicating that all atoms are involved in an isotope-exchange event. The slow rates of dissociation of the molecule could be independently measured and exhibit the same pH variation as the steady oxygen-isotope exchanges.[96,97,99–101,116]

What is important is that the overall rate of the oxygen-isotope exchange reaction is controlled by the *extent* that this metastable structure forms. This extent, in turn, reflects the strength of the M–μ_4-O bonds. A strong M–μ_4-O bond, as when $M = Ge^{IV}$, causes the *trans* Al^{III}–μ_4-O to weaken and allows more facile dissociation. A weak M–μ_4-O bond, as when $M = Ga^{II}$, causes the *trans* Al^{III}–μ_4-O to strengthen and suppresses intermediate formation. The extent of formation of the dimer-like structure controls the rates of observed isotope exchanges. At some point after the exchange, the metastable structure collapses back into the stable ε-Keggin form.

The key point for environmental chemists and geochemists is that the pathways for bond ruptures at the molecular scale involved concerted motions of many atoms, forming an unanticipated intermediate. The form could not be intuited by uninspired ab initio simulation of an imagined transition state using a cluster of atoms intended to capture the essence of the surface of an extended oxide. The energy landscape was too complicated to intuit and, in this case, the reaction pathway was identified by molecular dynamic simulations where the landscape could be sampled by a realistic ensemble of atoms. The discovery of this intermediate pathway demonstrates the power of coupling molecular-scale experiments to simulations of the same aqueous reaction.

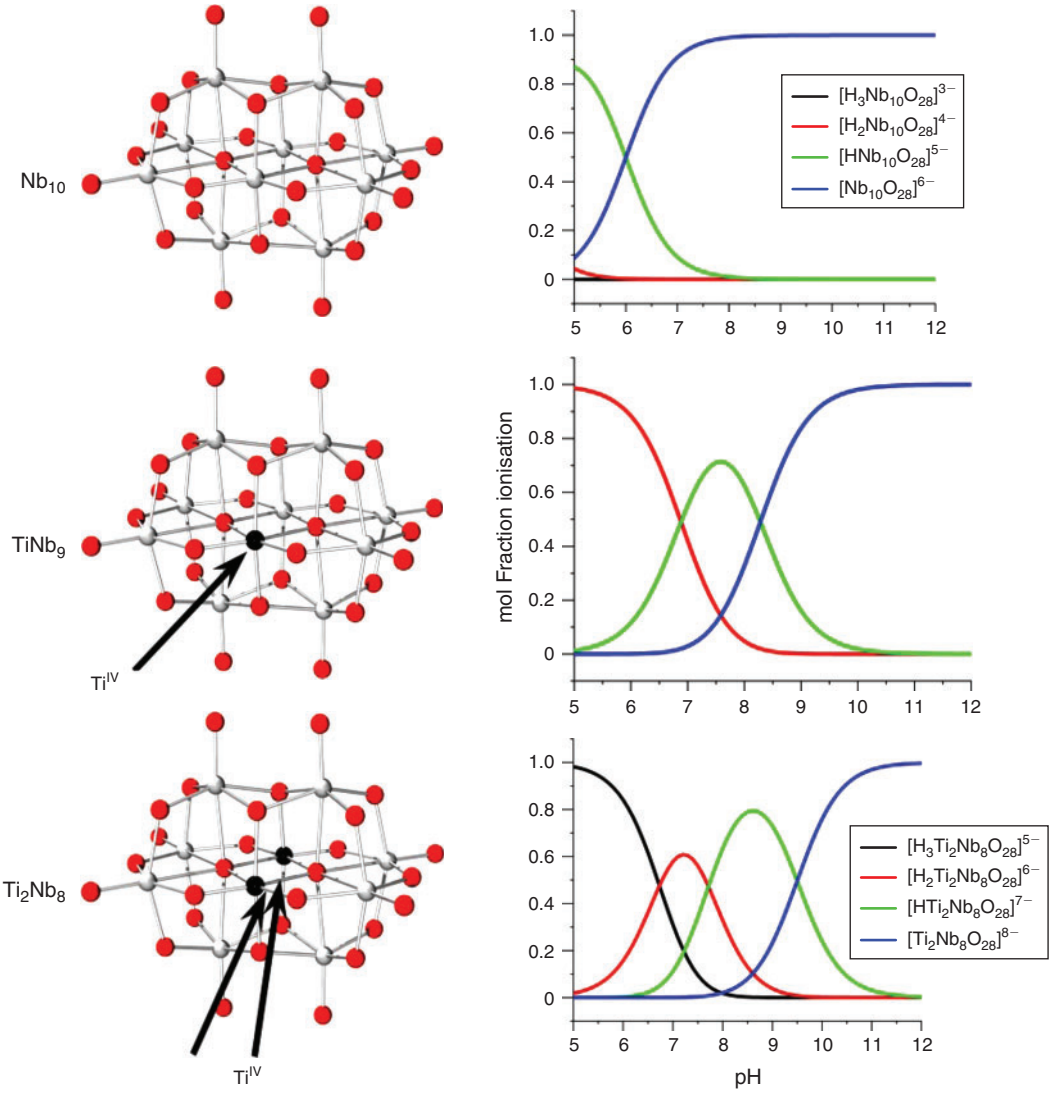

Fig. 10. Substitution of Ti^{IV} for Nb^{V} in the centre of these oxide structures changes the Brønsted acid–base properties,[96,97,99] which are manifested directly in the rates of oxygen-isotope-exchanges and dissociations (see Fig. 11, below). Substitutions are possible for many first-row transition metals, which gives the molecule distinctly different charges and proton affinities.

Decametalate anions

A second series of anionic molecules can show how oxide reactivity, at least for oxygen-isotopic exchanges, is affected by protonation. The decaniobate $[H_xNb_{10}O_{28}]^{(6-x)-}$ ion (Fig. 1, bottom) has seven structurally distinct oxygens in D_{2v} symmetry that react so slowly that oxygen-isotope exchanges can be followed at each site using ^{17}O NMR spectroscopy[96–101] over weeks. The effect of molecular charge on reaction kinetics and protonation were assessed by making a series of structures having the stoichiometries: $[H_xNb_{10}O_{28}]^{(6-x)-}$, $[H_xTiNb_9O_{28}]^{(7-x)-}$, and $[H_xTi_2Nb_8O_{28}]^{(8-x)-}$ by single-atom Ti^{IV} substitution for Nb^{V} in the centre of the molecule. These molecules are all made isotopically enriched in ^{17}O so that decreases in the ^{17}O NMR signal from each structural oxygen can be used to gauge rates of isotopic equilibration of that oxygen apart from all others in the structure.

As in the case for the MAl_{12} molecules, there is an inert oxygen site in the molecule that tells one when the molecule dissociates fully – it is a central μ_6-O with a sharp and distinct ^{17}O NMR signal[96–101] and, when the signal for this oxygen diminishes, it is clear that the molecule is dissociating. Slow diminution of the ^{17}O NMR signal for the central μ_6-O site unequivocally indicates that the decaniobate ion is slowly dissociating.

Experiments show that rates of dissociation increase with pH, at least for the decaniobate ion, and the dissociation rate is much slower than the rates of steady oxygen-isotope exchanges at the other six oxygen sites in the structure. The rates themselves differ by at least a factor of $\sim 10^4$ across the molecule. Each oxygen-isotope exchange rate varies similarly with pH (Fig. 9) and similarly to the pH dependence for dissociation of the structure.[99–100]

The shape of that pH dependency is important and is controlled by modifying the overall anionic charge of the molecule by heteroatom substitutions. The best estimate of the protonation chemistry is shown in Fig. 10, where it is perhaps unsurprising that proton affinities increase in the series: $[Nb_{10}O_{28}]^{6-}$, $[TiNb_9O_{28}]^{7-}$ and $[Ti_2Nb_8O_{28}]^{8-}$ along with overall anionic charge. What is a stunning result, and one that shed much light on processes at the mineral–solution interface, is that the pH variations of isotope-exchange rates for *all oxygens*

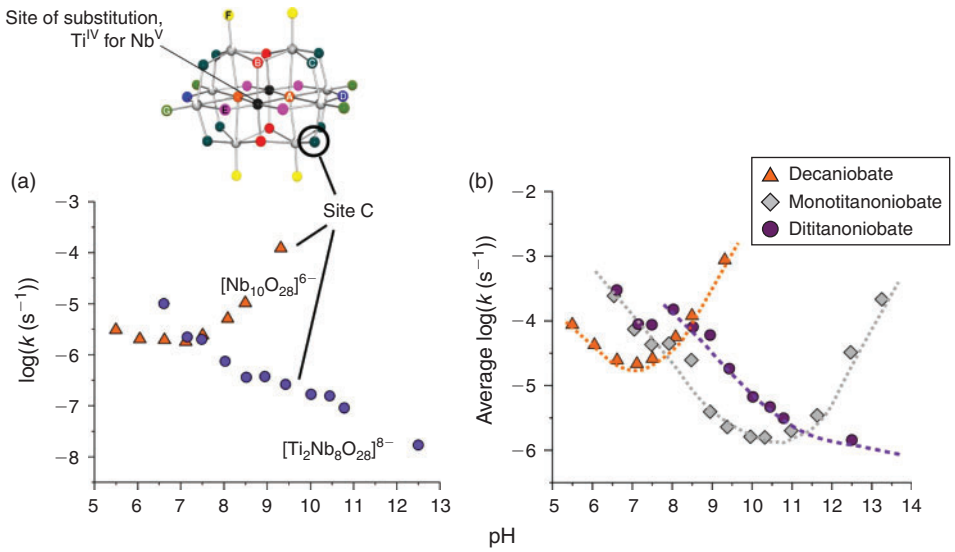

Fig. 11. The rates of oxygen-isotope-exchanges for one representative structural oxygen, Site C, in the decametalate structures. A single Ti^{IV} substitution (a) inverts the pH variation of rates for all oxygen sites in the structure. Note that the pH variation of the rates is broadly amphoteric (b), with rates accelerated by protons, hydroxyls and water molecules as nucleophiles, but that the relative importance of each pathway is determined by the overall proton affinity of that molecule, given by the charge of the unprotonated structure. The $[Nb_{10}O_{28}]^{6-}$ has the lowest relative proton affinity and has a hydroxide-enhanced pathway for oxygen-isotope exchanges. The $[Ti_2Nb_8O_{28}]^{8-}$ ion has the highest relative proton affinity (see Fig. 10) and exhibits only a proton-enhanced pathway for isotopic exchange. The pathways for oxygen-isotope exchange in the $[TiNb_9O_{28}]^{7-}$ ion is intermediate, with both prominent proton- and hydroxide-enhanced pathways evident.

reflect these average proton affinities. Stated differently, all reactive oxygens within a single molecule exhibit the same pH dependence to their rates of isotopic substitution. Different structural oxygens in molecules in the series: $[H_xNb_{10}O_{28}]^{(6-x)-}$, $[H_xTiNb_9O_{28}]^{(7-x)-}$ and $[H_xTi_2Nb_8O_{28}]^{(8-x)-}$, exhibit rates that are dominantly base-enhanced, proton-enhanced or a mixture of the two (Fig. 11), reflecting the *average* proton affinity of the structure. In all cases, the effect of proton affects *all* oxygens in the structure and the chemistry is broadly amphoteric, just like mineral dissolution rates. In other words, oxide clusters with 40 atoms already exhibit some of the important reactivity trends for hydrolytic reactions affecting extended mineral oxide surfaces.

To illustrate this point, in Fig. 11 are shown rates of isotopic exchange of the same oxygen, a μ_2-O site labelled 'C', in each of the $[H_xNb_{10}O_{28}]^{(6-x)-}$, $[H_xTiNb_9O_{28}]^{(7-x)-}$ and $[H_xTi_2Nb_8O_{28}]^{(8-x)-}$ molecules. The decaniobate ion is a weak base that picks up a proton at pH < 6, if at all, so it is primarily affected by base-enhanced hydrolysis; rates increase with pH. Each Ti^{IV} substitution into the molecule increases the net anionic charge, making it easier to protonate the molecule.

Note that the rates of oxygen-isotopic exchange of this oxygen in the $[Ti_2Nb_8O_{28}]^{8-}$ molecule increase as pH is reduced, indicating a dominantly proton-enhanced pathway for oxygen-isotope exchange. Again, remember that this pH dependence is observed for all reactive oxygens in the molecule, not just the one shown in the figure. In contrast, the rates of oxygen-isotope exchange of this oxygen in the $[Nb_{10}O_{28}]^{6-}$ molecule increases with pH, indicating a dominantly base-enhanced pathway for isotopic exchange (again, all reactive oxygens in the structure exhibit similar pH dependencies, as does dissociation of the molecule). Finally, the rates for the $[TiNb_9O_{28}]^{7-}$ molecule exhibit both proton- and hydroxy-enhanced pathways for isotopic exchange. There is a minimum in rates over a broad range in pH where the rates are not affected strongly by pH. This is a broad amphoteric chemistry.

Counterion choice also effects the oxygen-isotope exchange rates regiospecifically,[98] although we do not illustrate these effects with a figure. Also, the local effect on site reactivities of the Ti^{IV} substitution is surprisingly small – approximately a factor of two. The difference in rates of oxygen-isotope exchange at the same sites on either side of the $[TiNb_9O_{28}]^{7-}$ molecule are quite small and on the same order as that attributable to changes in the counterions. The oxygen site on one side would be near the Ti^{IV} substitution and the other would be distal.

These data indicate two points: (i) clusters of a few dozen atoms diverge sharply in reactivity from reaction pathways from small oligomers of the dimer and trimer size and (ii) the broad reactivity trends seem to resemble those found for mineral-dissolution studies of simple oxides and non-redox-sensitive minerals like feldspars. As we saw in the dissolution kinetics of mixed-composition solids, the effect of heteroatom addition on these 40–100 atom structures is averaged over the entire structure. Furthermore, all reactive oxygen sites exhibit the same pH variation in isotope-exchange rates, as though the atoms were reacting in concert. Finally, counterions affect some oxygens, but not all. These are exactly the broad reactivity trends we identified in the section *Some macroscopic reactivity trends*, above, for minerals undergoing hydrolysis and dissolution.

Broader lessons for mineral–interface chemistry

The results on these clusters have much to say to geochemists and chemists interested in natural interfacial chemistry. Even in cases where there is little similarity to mineral structures, these nanometre-sized ions allow direct comparison to simulations of the same reaction to assess the accuracy of theoretical

predictions. This alone makes them useful, however, there are some general rules that can be used to understand reactions at the nanometre-sized features on reactive mineral surfaces, such as kink sites.

To summarise the key observations on both the MAl_{12} and decametalate series of ions: (1) At the nanometre-size scale and in these densely packed structures, exchange rates at all oxygen sites in the molecule respond to changes in solution composition. At this scale, there is no such thing as an isolated functional group. (2) Heteroatom substitutions have profound effects on both the pH variation in rates and also the absolute magnitudes, but by the overall reactivity of the molecule. (3) Oxygen-isotope-exchange pathways and dissociation pathways are linked, at least in these densely packed structures. Finally, (4) the pH variation of rates is broadly amphoteric even in a 40-atom structure and reflective of the overall charge of the molecule.

We believe that there are rules about reaction pathways that can be extracted from studies of these large cations and anions. As in the case for the MAl_{12} cations, for both oxygen-isotope exchanges and dissociation, the condensed form of the stable molecule is in equilibrium with open metastable forms that are essential for the macroscopic isotope-exchange reaction to proceed. Each metastable structure has an appreciable lifetime and is not a transition state.

The metastable structures form by a similar set of steps identifiable in molecular-dynamic simulations: (1) The metastable form arises from detachment of a surface metal atom from an underlying, highly coordinated oxygen. In the decametalate structures, these highly coordinated oxygens are overbonded central μ_6-oxo. In the MAl_{12} series of cations these were the μ_4-oxo bonded to the central $Al(O)_4$ atom. (2) Formation of the intermediate(s) involves the concerted motions of many atoms, which is why heteroatom substitutions have an averaging effect on reactivity. This is most evident in the MAl_{12} series of molecules where Ga^{III} substitution suppresses the oxygen-exchange rates by over $\sim 10^7$ relative to the Ge^{IV}-centred molecule. The heteroatom affects the extent(s) that the metastable structure can be achieved. (3) Formation of the intermediate requires charge separation, which is why counterions affect the rates regiospecifically (Fig. 12). (4) Once formed, the newly undercoordinated metal in the loose intermediate adds an isotopically unique oxygen from solution. Internal shuffling of oxygen occurs at sites with low coordination numbers, such as the μ_2-O_2H_3 bridge in the MAl_{12} series of molecules. (5) Protons transfer rapidly among oxygens in the intermediate, which is why the average proton affinities are expressed in the rates, and not the protonation of a single oxygen.[102] Finally, the number and character of accessible metastable states reflects the symmetry and bonding in the stable form. For a molecule like $[Nb_{10}O_{28}]^{6-}$, with D_{2d} symmetry, there are many accessible intermediate structures. For the T_d symmetry of the MAl_{12} molecule, there are few. Thus it is probably not fruitful to speculate about the intermediates that might exist on the kink site on a dissolving mineral unless much (very much) is known about the atomic structure there.

It is easy to state the steps that control these reactions and we realise that they hide much detail, but they also tell geochemists about the appropriate scale for trying to understand their reactions, like mineral dissolution. If they are to be correct, molecular-scale simulations to understand oxygen-isotope exchanges or dissolution require extraordinary information about starting configurations and intermediate structures. The energy landscapes are much too complicated to intuit, or to be uncovered with simple static ab initio calculations, particularly if a truncated version of the system is employed to quicken the calculations (see Evans et al.[12]). These nanometre-sized ions are being used to advance theory across the field of solution chemistry (see van Eldik[103,104]).

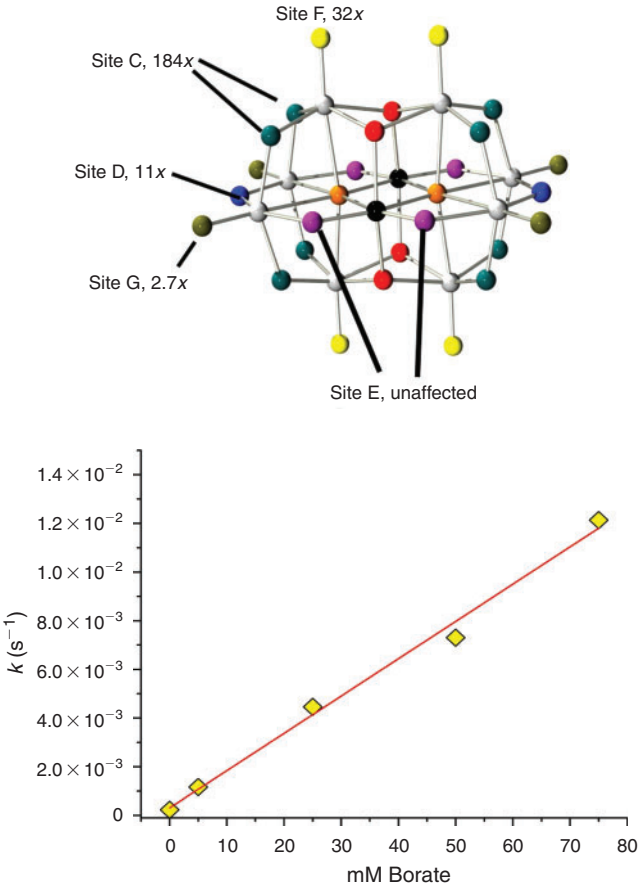

Fig. 12. Small amounts of borate ion, which exchanges oxygens in submillisecond timescales, affects the rates of steady oxygen-isotope exchanges for structural oxygens in the Ti_2Nb_8 ion ($[H_xTi_2Nb_8O_{28}]^{(8-x)-}$). Colours identify similar structural oxygens and the black atom indicates the site of substitution of Ti^{IV} for Nb^V, which are shown as white spheres. The numbers next to a particular oxygen (top) indicate the extent of increased lability in a 0.050-M borate solution relative to the case with no borate present. Rates increase linearly with borate concentration for Site C (a corner μ_2-oxo) (bottom).

This emphasis on metastable equilibration provides an obvious connection between pathways for oxygen-isotope exchanges and dissociation of the molecules. The rates of oxygen-isotope exchanges for a condensed structure like a feldspar will exhibit the same broad amphoteric variation with solution composition as the dissolution rates. The pathways are similar. This is also the same broad amphoteric variation of rates found in so many other classes of oxide reactions, such as oxygen-isotopic exchange into sugars, ester hydrolysis and pesticide hydrolysis. Water is the most common nucleophile simply because it is so abundant.

Acknowledgements

The author thanks John Chorover, Jim Rustad and three anonymous referees for careful reading of this text and helpful suggestions. Support was provided by the USA Department of Energy Office of Basic Energy Science grant DE-FG02-05ER15693.

References

[1] D. W. Margerum, G. R. Cayley, D. C. Weatherburn, G. K. Pagenkopf, Kinetics and mechanisms of complex formation and ligand exchange. *ACS Mono.* **1978**, *174*, 1.

[2] T. W. Swaddle, Ligand substitution dynamics in metal complexes, in *Physical Inorganic Chemistry: Reactions, Processes and Applications* (Ed. A. Bakac) **2010**, pp. 339–393 (Wiley: Hoboken, NJ).

[3] T. W. Swaddle, J. Rosenqvist, P. Yu, E. Bylaska, B. L. Phillips, W. H. Casey, Kinetic evidence for five-coordination in $AlOH(aq)^{2+}$ ion. *Science* **2005**, *308*, 1450. doi:10.1126/SCIENCE.1110231

[4] S. D. Kinrade, J. W. Del Nin, A. S. Schach, T. A. Sloan, K. L. Wilson, C. T. G. Knight, Stable five- and six-coordinated silicate anions in aqueous solution. *Science* **1999**, *285*, 1542. doi:10.1126/SCIENCE.285.5433.1542

[5] A. F. Panasci, C. A. Ohlin, S. J. Harley, W. H. Casey, Rates of water exchange on the $[Fe_4(OH)_2(hpdta)_2(H_2O)_4]^0$ molecule and its implications for geochemistry. *Inorg. Chem.* **2012**, *51*, 6731. doi:10.1021/IC300370Q

[6] L. Helm, A. E. Merbach, Inorganic and bioinorganic solvent exchange mechanisms. *Chem. Rev.* **2005**, *105*, 1923. doi:10.1021/CR030726O

[7] D. T. Richens, Ligand substitution reactions at inorganic centers. *Chem. Rev.* **2005**, *105*, 1961. doi:10.1021/CR030705U

[8] D. T. Richens, *The Chemistry of Aqua Ions* **1997** (Wiley: New York).

[9] L. Helm, G. M. Nicolle, A. E. Merbach, Water and proton exchange processes on metal ions. *Adv. Inorg. Chem.* **2005**, *57*, 327.

[10] A. G. Stack, P. Raiteri, J. D. Gale, Accurate rates of the complex mechanisms for growth and dissolution of minerals using a combination of rare-event theories. *J. Am. Chem. Soc.* **2012**, *134*, 11. doi:10.1021/JA204714K

[11] J. Wang, J. R. Rustad, W. H. Casey, Calculation of water-exchange rates on aqueous polynuclear clusters and at oxide-water interfaces. *Inorg. Chem.* **2007**, *46*, 2962. doi:10.1021/IC070079+

[12] R. J. Evans, J. R. Rustad, W. H. Casey, Calculating geochemical reaction pathways – exploration of the inner-sphere water exchange mechanism in $Al(H_2O)_6^{3+}(aq) + nH_2O$ with ab initio calculations and molecular dynamics. *J. Phys. Chem. A* **2008**, *112*, 4125. doi:10.1021/JP7116888

[13] F. P. Rotzinger, Treatment of substitution and rearrangement mechanisms of transition metal complexes with quantum chemical methods. *Chem. Rev.* **2005**, *105*, 2003. doi:10.1021/CR030715V

[14] E. Balogh, et al., Rates of ligand exchange between $>Fe^{III}\text{-}OH_2$ functional groups on a nanometer-size aqueous cluster and bulk solution. *Inorg. Chem.* **2007**, *46*, 7087. doi:10.1021/IC7009308

[15] D. Lieb, et al., Water exchange reactivity and stability of cobalt polyoxometalates under catalytically relevant pH conditions: insight into water oxidation catalysis. *Inorg. Chem.* **2011**, *50*, 9053. doi:10.1021/IC201243N

[16] C. A. Ohlin, et al., Rates of water exchange for two cobalt(II) heteropolyoxotungstate compounds in aqueous solution. *Chemistry* **2011**, *17*, 4408. doi:10.1002/CHEM.201003550

[17] T. W. Swaddle, A. E. Merbach, High-pressure oxygen-17 Fourier transform nuclear magnetic resonance spectroscopy. Mechanism of water exchange on iron(III) in acidic aqueous solution. *Inorg. Chem.* **1981**, *20*, 4212. doi:10.1021/IC50226A036

[18] S. F. Lincoln, D. T. Richens, A. G. Sykes, Metal aqua ions. *Compr. Coordin. Chem. II* **2004**, *1*, 515. doi:10.1016/B0-08-043748-6/01055-0

[19] L. Spiccia, W. H. Casey, Synthesis of experimental models for molecular inorganic geochemistry – a review with examples. *Geochim. Cosmochim. Acta* **2007**, *71*, 5590. doi:10.1016/J.GCA.2007.03.041

[20] L. Spiccia, Homopolynuclear and heteropolynuclear Rh(III) aqua ions – a review. *Inorg. Chim. Acta* **2004**, *357*, 2799. doi:10.1016/J.ICA.2003.12.036

[21] S. J. Crimp, et al., Synthesis and characterization of rhodium(III)-chromium(III) heterotrinuclear aqua ions. *J. Chem. Soc., Dalton Trans.* **1998**, 375. doi:10.1039/A707088H

[22] L. Spiccia, et al., Hydrolytic polymerization of rhodium(III). Characterization of various forms of a trinuclear aqua ion. *J. Chem. Soc., Dalton Trans.* **1997**, 4603. doi:10.1039/A704694D

[23] A. Drljaca, et al., Kinetics of water exchange on the hydrolytic doubly hydroxo-bridged rhodium(III) dimer. *Inorg. Chem.* **1996**, *35*, 985. doi:10.1021/IC950423F

[24] A. Drljaca, L. Spiccia, Early stages of the hydrolysis of chromium (III) in aqueous solution – XII. Kinetics of cleavage of the trimer and tetramer in acidic solution. *Polyhedron* **1996**, *15*, 4373. doi:10.1016/0277-5387(96)00209-4

[25] A. Drljaca, L. Spiccia, Early stages of the hydrolysis of chromium (III) in aqueous solution-XI. Kinetics of formation of hexamer from trimer and tetramer from monomer and trimer. *Polyhedron* **1996**, *15*, 2875. doi:10.1016/0277-5387(95)00594-3

[26] S. J. Crimp, L. Spiccia, Kinetic and thermodynamic studies of intramolecular rearrangement and cleavage of the heterobinuclear aqua ion, $[(H_2O)_4Rh(\mu\text{-}OH)_2Cr(OH_2)_4]^{4+}$. *J. Chem. Soc., Dalton Trans.* **1996**, 1051. doi:10.1039/DT9960001051

[27] A. Drljaca, L. Spiccia, Early stages of the hydrolysis of chromium (III) in aqueous solution-X. Kinetics of formation of trimer from monomer and dimer. *Polyhedron* **1995**, *14*, 1653. doi:10.1016/0277-5387(94)00429-I

[28] S. J. Crimp, L. Spiccia, Characterization of three active rhodium(III) hydroxides. *Aust. J. Chem.* **1995**, *48*, 557. doi:10.1071/CH9950557

[29] S. J. Crimp, et al., Early stages of the hydrolysis of chromium(III) in aqueous solution. 9. Kinetics of water exchange on the hydrolytic dimer. *Inorg. Chem.* **1994**, *33*, 465. doi:10.1021/IC00081A012

[30] L. Spiccia, W. Marty, Early stages of the hydrolysis of chromium(III) in aqueous solution. VI. Kinetics of intramolecular interconversion between singly and doubly bridged hydrolytic dimers. *Polyhedron* **1991**, *10*, 619. doi:10.1016/S0277-5387(00)83621-9

[31] L. Spiccia, Early stages of the hydrolysis of chromium(III) in aqueous solution. 7. Kinetics of cleavage of the hydrolytic dimer in acidic solution. *Polyhedron* **1991**, *10*, 1865. doi:10.1016/S0277-5387(00)86047-7

[32] M. R. Grace, L. Spiccia, Early stages of the hydrolysis of chromium (III) in aqueous solution. VIII. Kinetics of dimerization of deprotonated forms of doubly bridged dimer. *Polyhedron* **1991**, *10*, 2389. doi:10.1016/S0277-5387(00)86200-2

[33] R. Cervini, G. D. Fallon, L. Spiccia, Hydrolytic polymerization of rhodium(III). 1. Preparation, solution studies, and x-ray structure of the doubly bridged dimer $[(H_2O)_4Rh(\mu\text{-}OH)_2Rh(OH_2)_4](dmtos)_4{\cdot}8H_2O$. *Inorg. Chem.* **1991**, *30*, 831. doi:10.1021/IC00004A042

[34] H. Stuenzi, L. Spiccia, F. P. Rotzinger, W. Marty, Early stages of the hydrolysis of chromium(III) in aqueous solution. 4. The stability constants of the hydrolytic dimer, trimer, and tetramer at 25 °C and I = 1.0 M. *Inorg. Chem.* **1989**, *28*, 66. doi:10.1021/IC00300A015

[35] T. Merakis, L. Spiccia, Early stages of the hydrolysis of chromium (III) in aqueous solution. V. Measurement of the equilibrium between singly and doubly bridged dimer. *Aust. J. Chem.* **1989**, *42*, 1579. doi:10.1071/CH9891579

[36] F. P. Rotzinger, H. Stuenzi, W. Marty, Early stages of the hydrolysis of chromium(III) in aqueous solution. 3. Kinetics of dimerization of the deprotonated aqua ion. *Inorg. Chem.* **1986**, *25*, 489. doi:10.1021/IC00224A019

[37] F. P. Rotzinger, W. Marty, A unified interpretation of kinetic data on the acid-induced cleavage and of product-analysis data on spontaneous cleavage of the mono-ol cation μ-hydroxo-bis[pentaamminecobalt(III)]($[(NH_3)_5CoOHCo(NH_3)_5]^{5+}$). *Helv. Chim. Acta* **1985**, *68*, 1914. doi:10.1002/HLCA.19850680715

[38] H. Stünzi, F. P. Rotzinger, W. Marty, Early stages of the hydrolysis of chromium(III) in aqueous solution. 2. Kinetics and mechanism of the interconversion between two tetrameric species. *Inorg. Chem.* **1984**, *23*, 2160. doi:10.1021/IC00182A035

[39] F. P. Rotzinger, W. Marty, Activated ligand substitution in bridged complexes. 1. Base hydrolysis and structure of (+-)-(m-amido)-cis,-cis-tetrakis(1,2-ethanediamine)diamminedicobalt(III) pentanitrate dihydrate. *Inorg. Chem.* **1983**, *22*, 3593. doi:10.1021/IC00166A022

[40] A. F. Panasci, J. G. McAlpin, C. A. Ohlin, S. Christensen, J. C. Fettinger, R. D. Britt, J. R. Rustad, W. H. Casey, Cooperation between bound waters and hydroxyls in controlling isotope-

exchange rates. *Geochim. Cosmochim. Acta* **2012**, *78*, 18. doi:10.1016/J.GCA.2011.10.041

[41] T. W. Swaddle, Silicate complexes of aluminum(III) in aqueous systems. *Coord. Chem. Rev.* **2001**, *219–221*, 665. doi:10.1016/S0010-8545(01)00362-9

[42] T. W. Swaddle, J. Salerno, P. A. Tregloan, Aqueous aluminates, silicates, and aluminosilicates. *Chem. Soc. Rev.* **1994**, *23*, 319. doi:10.1039/CS9942300319

[43] S. J. Brudenell, S. J. Crimp, J. K. E. Higgs, K. Moubaraki, K. S. Murray, L. Spiccia, Binuclear chromium(III) complexes bridged by hydroxide and acetate groups. *Inorg. Chim. Acta* **1996**, *247*, 35. doi:10.1016/0020-1693(95)04827-8

[44] M. R. Grace, L. Spiccia, Kinetics of anation of Cr(III) hydrolytic oligomers: reaction of dimer with sulfate. *Inorg. Chim. Acta* **1993**, *213*, 103. doi:10.1016/S0020-1693(00)83820-7

[45] A. Drljaca, J. R. Anderson, L. Spiccia Turney, Intercalation of montmorillonite with individual chromium(III) hydrolytic oligomers. *Inorg. Chem.* **1992**, *31*, 4894. doi:10.1021/IC00049A033

[46] S. J. Crimp, G. D. Fallon, L. Spiccia, Synthesis and x-ray structure of a chromium(III)-rhodium(III) heterometallic hydrolytic dimer: $[(H_2O)_4Rh(\mu\text{-}OH)_2Cr(OH_2)_4](Me_3C_6H_2SO_3)_4\cdot 4H_2O$. *J. Chem. Soc. Chem. Commun.* **1992**, *1992*, 197. doi:10.1039/C39920000197

[47] L. Spiccia, W. Marty, The fate of active chromium hydroxide, $Cr(OH)_3\cdot 3H_2O$, in aqueous suspension. Study of the chemical changes involved in its aging. *Inorg. Chem.* **1986**, *25*, 266. doi:10.1021/IC00223A007

[48] J. Springborg, Hydroxo-bridged complexes of chromium(III), cobalt (III), rhodium(III), and iridium(III). *Adv. Inorg. Chem.* **1988**, *32*, 55.

[49] A. Müller, F. Peters, M. T. Pope, D. Gatteschi, Polyoxometalates: very large clusters – Nanoscale magnets. *Chem. Rev.* **1998**, *98*, 239. doi:10.1021/CR9603946

[50] M. T. Pope, *Heteropoly and Isopoly Oxometalates* **1983** (Springer: Berlin).

[51] A. Müller, E. Diemann, S. Q. N. Shah, C. Kuhlmann, M. Letzel, Soccer-playing metal oxide giant spheres: a first step towards patterning structurally well defined nano-object collectives. *Chem. Commun.* **2002**, *2002*, 440. doi:10.1039/B110917K

[52] M. T. Pope, A. Müller (Eds), *Polyoxometalates: from platonic solids to anti-retroviral activity. Topics in Molecular Organization and Engineering, Vol. 10* **1994** (Springer: Netherlands).

[53] C. L. Hill, Polyoxometalates: reactivity. *Compr. Coordin. Chem. II* **2004**, *4*, 679. doi:10.1016/B0-08-043748-6/03036-X

[54] M. Filowitz, R. K. C. Ho, W. G. Klemperer Shum, Oxygen-17 nuclear magnetic resonance spectroscopy of polyoxometalates. 1. Sensitivity and resolution. *Inorg. Chem.* **1979**, *18*, 93. doi:10.1021/IC50191A021

[55] C. J. Besecker, W. G. Klemperer, D. J. Maltbie, D. A. Wright,, Oxygen-17 nuclear magnetic resonance spectroscopy of polyoxometalates. 2. Heteronuclear decoupling of quadrupolar nuclei. *Inorg. Chem.* **1985**, *24*, 1027. doi:10.1021/IC00201A013

[56] L. Pettersson, I. Andersson, F. Taube, I. Toth, M. Hashimoto, O. W. Howarth, 17O NMR study of aqueous peroxoisopolymolybdate equilibria at lower peroxide/Mo ratios. *Dalton Trans.* **2003**, 146. doi:10.1039/B206396B

[57] J. J. Hastings, O. W. Howarth, A tungsten-183, proton and oxygen-17 nuclear magnetic resonance study of aqueous isopolytungstates. *J. Chem. Soc., Dalton Trans.* **1992**, *2*, 209. doi:10.1039/DT9920000209

[58] O. W. Howarth, P. Kelly, Intramolecular oxygen exchange in the heptamolybdate(VI) isopolyanion. *J. Chem. Soc. Chem. Commun.* **1988**, 1236. doi:10.1039/C39880001236

[59] A. T. Harrison, O. W. Howarth, Oxygen exchange and protonation of polyanions: a multinuclear magnetic resonance study of tetradecavanadophosphate(9-) and decavanadate(6-). *J. Chem. Soc., Dalton Trans.* **1985**, *9*, 1953. doi:10.1039/DT9850001953

[60] R. K. Murmann, M. E. Shelton, Isotopic oxygen studies on aqueous molybdenum(IV). *J. Amer. Chem. Soc.* **1980**, *102*, 3984. doi:10.1021/JA00531A068

[61] K. R. Rodgers, R. K. Murmann, E. O. Schlemper, M. E. Shelton, Rates of isotopic oxygen exchange with solvent and oxygen atom transfer involving $[Mo_3O_4(OH_2)_9]^{4+}$. *Inorg. Chem.* **1985**, *24*, 1313. doi:10.1021/IC00203A011

[62] W. H. Casey, T. W. Swaddle, Why small? The use of small inorganic clusters to understand mineral surface and dissolution reactions in geochemistry. *Rev. Geophys.* **2003**, *41*, 1008. doi:10.1029/2002RG000118

[63] M. R. North, M. A. Fleischer, T. W. Swaddle, Precipitation from alkaline aqueous aluminosilicate solutions. *Can. J. Chem.* **2001**, *79*, 75. doi:10.1139/V00-182

[64] M. R. North, T. W. Swaddle, Kinetics of silicate exchange in alkaline aluminosilicate solutions. *Inorg. Chem.* **2000**, *39*, 2661. doi:10.1021/IC0000707

[65] E. Vallazza, A. D. Bain, T. W. Swaddle, Dynamics of silicate exchange in highly alkaline potassium silicate solutions. *Can. J. Chem.* **1998**, *76*, 183.

[66] C. T. G. Knight, R. J. Balec, S. D. Kinrade, The structure of silicate anions in aqueous alkaline solutions. *Angew. Chem. Int. Ed.* **2007**, *46*, 8148. doi:10.1002/ANIE.200702986

[67] S. D. Kinrade, J. C. H. Donovan, A. S. Schach, C. T. G. Knight, Two substituted cubic octameric silicate cages in aqueous solution. *J. Chem. Soc., Dalton Trans.* **2002**, 1250. doi:10.1039/B107758A

[68] S. D. Kinrade, C. T. G. Knight, D. L. Pole, R. T. Syvitski, Silicon-29 NMR studies of tetraalkylammonium silicate solutions. 2. Polymerization kinetics. *Inorg. Chem.* **1998**, *37*, 4278. doi:10.1021/IC971630D

[69] S. D. Kinrade, C. T. G. Knight, D. L. Pole, R. T. Syvitski, Silicon-29 NMR studies of tetraalkylammonium silicate solutions. 1. Equilibria, ^{29}Si chemical shifts, and ^{29}Si relaxation. *Inorg. Chem.* **1998**, *37*, 4272. doi:10.1021/IC971629E

[70] S. D. Kinrade, K. Marat, C. T. G. Knight, Longitudinal ^{29}Si nuclear magnetic relaxation in aqueous alkali-metal silicate solutions revisited. *J. Phys. Chem.* **1996**, *100*, 18351. doi:10.1021/JP9618845

[71] S. D. Kinrade, Oxygen-17 NMR study of aqueous potassium silicates. *J. Phys. Chem.* **1996**, *100*, 4760. doi:10.1021/JP952683O

[72] S. D. Kinrade, D. L. Pole, Effect of alkali-metal cations on the chemistry of aqueous silicate solutions. *Inorg. Chem.* **1992**, *31*, 4558. doi:10.1021/IC00048A023

[73] S. D. Kinrade, T. W. Swaddle, Silicon-29 NMR studies of aqueous silicate solutions. 1. Chemical shifts and equilibria. *Inorg. Chem.* **1988**, *27*, 4253. doi:10.1021/IC00296A034

[74] S. D. Kinrade, T. W. Swaddle, Silicon-29 NMR studies of aqueous silicate solutions. 2. Transverse silicon-29 relaxation and the kinetics and mechanism of silicate polymerization. *Inorg. Chem.* **1988**, *27*, 4259. doi:10.1021/IC00296A035

[75] S. D. Kinrade, T. W. Swaddle, Mechanisms of longitudinal silicon-29 nuclear magnetic relaxation in aqueous alkali-metal silicate solutions. *J. Am. Chem. Soc.* **1986**, *108*, 7159. doi:10.1021/JA00283A004

[76] S. D. Kinrade, T. W. Swaddle, Aqueous silicate exchange dynamics and silicon-29 nuclear magnetic relaxation: the importance of protonation equilibriums. *J. Chem. Soc. Chem. Commun.* **1986**, 120. doi:10.1039/C39860000120

[77] W. H. Casey, G. Sposito, On the temperature dependence of mineral dissolution rates. *Geochim. Cosmochim. Acta* **1992**, *56*, 3825. doi:10.1016/0016-7037(92)90173-G

[78] T. Schneppensieper, S. Seibig, A. Zahl, P. Tregloan, R. van Eldik, Influence of chelate effects on the water-exchange mechanism of polyaminecarboxylate complexes of iron(III). *Inorg. Chem.* **2001**, *40*, 3670. doi:10.1021/IC001304P

[79] J. Maigut, R. Meier, A. Zahl, R. van Eldik, Triggering water exchange mechanisms via chelate architecture. Shielding of transition metal centers by aminopolycarboxylate spectator ligands. *J. Am. Chem. Soc.* **2008**, *130*, 14 556. doi:10.1021/JA802842Q

[80] T. Schneppensieper, A. Zahl, R. van Eldik, Water exchange controls the complex-formation mechanism of water-soluble iron(III) porphyrins: conclusive evidence for dissociative water exchange from a high-pressure ^{17}O NMR study. *Angew. Chem. Int. Ed.* **2001**, *40*, 1678. doi:10.1002/1521-3773(20010504)40:9<1678::AID-ANIE16780>3.0.CO;2-A

[81] L. Babcock, R. Pizer, Dynamics of boron acid complexation reactions: formation of the 1 : 1 boron acid-ligand complexes. *Inorg. Chem.* **1980**, *19*, 56. doi:10.1021/IC50203A013

[82] K. Yoshino, M. Kotaka, M. Okamoto, H. Kakihana, 11B-NMR study of the complex formation of borate with catechol and L-dopa. *Bull. Chem. Soc. Jpn.* **1979**, *52*, 3005. doi:10.1246/BCSJ.52.3005

[83] R. Pizer, P. J. Ricatto, C. A. Tihal, Thermodynamics of several boron acid complexation reactions studied by variable-temperature ^{1}H- and ^{11}B-NMR spectroscopy. *Polyhedron* **1993**, *12*, 2137. doi:10.1016/S0277-5387(00)84377-6

[84] R. Pizer, C. A. Tihal, Mechanism of boron acid/polyol complex formation. Comments on the trigonal/tetrahedral interconversion on boron. *Polyhedron* **1996**, *15*, 3411. doi:10.1016/0277-5387(96)00042-3

[85] M. Ishihara, Y. Mouri, S. Funahashi, M. Tanaka, Mechanistic study of the complex formation of boric acid. *Inorg. Chem.* **1991**, *30*, 2356. doi:10.1021/IC00010A025

[86] S. Kagawa, K.-I. Sugimoto, S. Funahashi, Kinetic study on complexation of boric acid with 4-isopropyltropolone in non-aqueous solvents. *Inorg. Chim. Acta* **1995**, *231*, 115. doi:10.1016/0020-1693(94)04340-2

[87] R. Pizer, L. Babcock, Mechanism of the complexation of boron acids with catechol and substituted catechols. *Inorg. Chem.* **1977**, *16*, 1677. doi:10.1021/IC50173A021

[88] A. Crumbliss, A.-M. Albrecht-Gary, Coordination chemistry of siderophores: thermodynamics and kinetics of iron chelation and release, in *Metal Ions in Biological Systems* (Eds A. Sigal, H. Sigal) **1998** (Marcel Dekker: New York).

[89] J. G. Hering, M. M. Morel Francois, Slow complexation reactions in seawater. *Geochim. Cosmochim. Acta* **1989**, *53*, 611. doi:10.1016/0016-7037(89)90004-5

[90] F. G. Kari, W. Giger, Modeling the photochemical degradation of ethylenediaminetetraacetate in the River Glatt. *Environ. Sci. Technol.* **1995**, *29*, 2814. doi:10.1021/ES00011A018

[91] B. Nowack, H. Xue, L. Sigg, Influence of natural and anthropogenic ligands on metal transport during infiltration of river water to groundwater. *Environ. Sci. Technol.* **1997**, *31*, 866. doi:10.1021/ES960556F

[92] A. F. Wallace, G. V. Gibbs, P. M. Dove, Influence of ion-associated water on the hydrolysis of Si-O bonded nteractions. *J. Phys. Chem. A* **2010**, *114*, 2534. doi:10.1021/JP907851U

[93] A. Czap, N. I. Neuman, T. W. Swaddle, Electrochemistry and homogeneous self-exchange kinetics of the aqueous 12-tungstoaluminate (5-/6-) couple. *Inorg. Chem.* **2006**, *45*, 9518. doi:10.1021/IC060527Y

[94] J. R. Rustad, J. S. Loring, W. H. Casey, Oxygen-exchange pathways in aluminum polyoxocations. *Geochim. Cosmochim. Acta* **2004**, *68*, 3011. doi:10.1016/J.GCA.2003.12.021

[95] W. H. Casey, J. R. Rustad, Reaction dynamics, molecular clusters and aqueous geochemistry. *Annu. Rev. Earth Sci.* **2007**, *35*, 21. doi:10.1146/ANNUREV.EARTH.35.031306.140117

[96] E. M. Villa, C. A. Ohlin, J. R. Rustad, W. H. Casey, Isotope-exchange dynamics in isostructural decametalates with profound differences in reactivity. *J. Am. Chem. Soc*. **2009**, *131*, 16 488. doi:10.1021/JA905166C

[97] E. M. Villa, C. A. Ohlin, W. H. Casey, Adding reactivity to structure 2: oxygen-isotope-exchange rates in three isostructural oxide ions. *Am. J. Sci.* **2010**, *310*, 629. doi:10.2475/07.2010.03

[98] E. M. Villa, C. A. Ohlin, W. H. Casey, Borate accelerates oxygen-isotope exchange for polyoxoniobate ions in water. *Chemistry* **2010**, *16*, 8631. doi:10.1002/CHEM.201000946

[99] E. M. Villa, C. A. Ohlin, W. H. Casey, Oxygen-isotope exchange rates for three isostructural polyoxometalate ions. *J. Am. Chem. Soc.* **2010**, *132*, 5264. doi:10.1021/JA100490N

[100] E. M. Villa, C. A. Ohlin, E. Balogh, T. M. Anderson, M. D. Nyman, W. H. Casey, Reaction dynamics of the decaniobate ($[H_xNb_{10}O_{28}]^{(6-x)-}$) ion in water. *Angew. Chem. Int. Ed.* **2008**, *47*, 4844. doi:10.1002/ANIE.200801125

[101] E. M. Villa, C. A. Ohlin, E. Balogh, T. A. Anderson, M. Nyman, W. H. Casey, Adding reactivity to structure – reaction dynamics in a nanometer-size oxide ion in water. *Am. J. Sci.* **2008**, *308*, 942. doi:10.2475/08.2008.03

[102] J. R. Rustad, W. H. Casey, Metastable structures and isotope exchange reactions in polyoxometalate ions provide a molecular view of oxide dissolution. *Nat. Mater.* **2012**, *11*, 223. doi:10.1038/NMAT3203

[103] R. van Eldik (Ed.) *Advances in Inorganic Chemistry* **2010**, Vol. 62 (Academic Press: San Diego, CA).

[104] J. R. Rustad, Elementary reactions in polynuclear ions and aqueous-mineral interfaces: a new geology, in *Advances in Inorganic Chemistry* (Ed. R. van Eldik) **2010**, pp. 391–436 (Academic Press: San Diego, CA).

[105] W. H. Casey, On the relative dissolution rates of some oxide and orthosilicate minerals. *J. Colloid Interface Sci.* **1991**, *146*, 586. doi:10.1016/0021-9797(91)90225-W

[106] H. Stuenzi, W. Marty, Early stages of the hydrolysis of chromium (III) in aqueous solution. 1. Characterization of a tetrameric species. *Inorg. Chem.* **1983**, *22*, 2145. doi:10.1021/IC00157A012

[107] T. V. Rowland, *Oxygen-17 NMR studies of the rate of water exchange from partially complexed nickel ion* **1975**, Ph.D. thesis, University of California, Berkeley.

[108] J. Burgess, *Metal Ions in Solution* **1978** (Ellis-Horwood Limited: Chichester, UK).

[109] J. Burgess, *Ions in Solution: Basic Principles of Chemical Interactions* **1988** (Ellis-Horwood Limited: Chichester, UK).

[110] D. W. Margerum, H. M. Rosen, The effect of coordinated ligands on the rate of replacement of bound water by ammonia in nickel(II) complexes. *J. Am. Chem. Soc.* **1967**, *89*, 1088. doi:10.1021/JA00981A009

[111] R. G. Wilkins, *The Study of Kinetics and Mechanism of Reactions of Transition Metal Complexes*. **1974** (VCH: New York).

[112] R. G. Wilkins, *The Study of Kinetics and Mechanism of Reactions of Transition Metal Complexes*, 2nd edn **1991** (VCH: New York).

[113] W. H. Casey, H. R. Westrich, Control of dissolution rates of orthosilicate minerals by divalent metal-oxygen bonds. *Nature* **1992**, *355*, 157. doi:10.1038/355157A0

[114] O. S. Pokrovsky, J. Schott, Surface chemistry and dissolution kinetics of divalent metal carbonates. *Environ. Sci. Technol.* **2002**, *36*, 426. doi:10.1021/ES010925U

[115] K. Hachiya, M. Sasaki, Y. Saruta, N. Mikami Yasunaga, Static and kinetic studies of adsorption-desorption of metal ions on a γ-alumina surface. 1. Static study of adsorption-desorption. *J. Phys. Chem.* **1984**, *88*, 23. doi:10.1021/J150645A007

[116] C. A. Ohlin, et al., The dissolution of insulating oxides at the molecular scale. *Nat. Mater.* **2010**, *9*, 11. doi:10.1038/NMAT2585

[117] W. H. Casey, Large aqueous aluminum-hydroxide molecules. *Chem. Rev.* **2006**, *106*, 1. doi:10.1021/CR040095D

[118] J. Rowsell, L. F. Nazar, Speciation and thermal transformation in alumina sols: structures of the polyhydroxyoxoaluminum cluster $[Al_{30}O_8(OH)_{56}(H_2O)_{26}^{18+}$ and its δ-Keggin moiete. *J. Am. Chem. Soc.* **2000**, *122*, 3777. doi:10.1021/JA993711+

[119] L. Allouche, C. Gerardin, T. Loiseau, G. Ferey, F. Taulelle, Al_{30}: a giant aluminum polycation. *Angew. Chem. Int. Ed.* **2000**, *39*, 511. doi:10.1002/(SICI)1521-3773(20000204)39:3<511::AID-ANIE511>3.0.CO;2-N

[120] W. H. Casey, J. R. Rustad, L. Spiccia, Minerals as molecules – use of aqueous oxide and hydroxide clusters to understand geochemical reactions. *Chemistry* **2009**, *15*, 4496. doi:10.1002/CHEM.200802636

[121] H. R. Westrich, R. T. Cygan, W. H. Casey, C. Zemitis, G. W. Arnold, The dissolution kinetics of mixed-cation orthosilicate minerals. *Am. J. Sci.* **1993**, *293*, 869. doi:10.2475/AJS.293.9.869